Atmospheric Environment: X 3 (2019) 100042

Contents lists available at ScienceDirect

Atmospheric Environment: X

journal homepage: www.journals.elsevier.com/atmospheric-environment-x

Inclusion of CO_2 flux modelling in an urban canopy layer model and an evaluation over an old European city centre

Marine Goret[a,*], Valéry Masson[a], Robert Schoetter[a], Marie-Pierre Moine[b]

[a] CNRM, Université de Toulouse, Météo-France, CNRS, 42 avenue Gaspard Coriolis, 31057, Cedex 1, Toulouse, France
[b] CECI, Université de Toulouse, CERFACS/CNRS, 42 avenue Gaspard Coriolis, 31057, Cedex 1, Toulouse, France

ARTICLE INFO

Keywords:
CO_2fluxes
Eddy covariance
Cities
Urban canopy layer model
Model evaluation

ABSTRACT

In the context of climate change, the reduction of greenhouse gas emissions is a global concern. Recent publications estimate that 30–40% of total anthropogenic greenhouse gases are directly emitted by urban areas. This paper focuses on CO_2, which is the main anthropogenic greenhouse gas, and presents an implementation of CO_2 flux modelling in urban areas within the urban canopy model Town Energy Balance (TEB). Highly weather-dependent contributors to CO_2 fluxes (buildings and vegetation) are explicitly modelled by TEB using the Building Energy Model (BEM) for buildings and Interactions between Soil, Biosphere and Atmosphere (ISBA) for urban vegetation. This approach allows the impacts of the urban microclimate on CO_2 fluxes to be simulated. Non-weather-dependent contributors (traffic and human respiration) are simulated using simpler approaches. A sensitivity study applied to the centre of Toulouse, France, highlights the relevance of detailed input data related to traffic, building use and human behaviour to simulate accurate CO_2 fluxes. The results show that traffic (48.5%) and buildings (42%) are the main contributors to the annual mean CO_2 flux. A comparison of the model results with independent eddy-covariance flux data shows good agreement with a root mean square error of 15.3 μmol m^{-2} s^{-1} and demonstrates that the model is able to reproduce seasonally averaged daily cycles of CO_2 fluxes. In future studies, this model can be used to quantify the impacts on CO_2 fluxes of different urban development scenarios such as urban expansion, changes in urban form, changes in practices related to the heating of buildings or urban greening strategies.

1. Introduction

The quantity of anthropogenic greenhouse gases (GHGs) released into the atmosphere has greatly increased during the past decades. It increased by 2.2% per year between 2000 and 2010 to reach approximately 50 $GtCO_2$ equivalent per year in 2010 (Edenhofer et al., 2014). The contribution of cities is important because the GHGs they locally emit represent 30–40% of the total anthropogenic GHGs (Satterthwaite, 2008). The contribution of cities is even larger if we also consider remote emissions (for example, GHGs released in rural areas for the production of electricity used in cities). Hereafter, we aim to quantify only local emissions because the present study uses in-situ data from a field campaign. This paper focuses on the main anthropogenic GHG, CO_2.

Building inventories are a reference method used to estimate CO_2 emissions/uptake (Moriwaki and Kanda, 2004). Such inventories are based on bottom-up approaches, in which emission factors are applied to activity data or fuel consumption in different sectors. Inventories are widely used, and there exist guidelines to construct official inventories (Eggleston et al., 2006; U.S. Environmental Protection Agency, 2016). Inventory methods perform well when estimating CO_2 emissions related to fuel combustion but are less relevant when evaluating the vegetative contribution to CO_2 fluxes. Even with a precise characterisation of the vegetation (e.g. biomass density, evergreen/deciduous and high/low vegetation), only a coarse estimation of CO_2 emissions and uptake can be made. Because vegetation growth and behaviour are strongly weather dependent, a more precise estimate would require knowing the weather conditions, which are not considered in inventory methods. Another drawback of inventory methods is that they are sensitive to the quality of the baseline data and to their spatial and temporal resolutions. Inventories are usually retrieved at an annual scale and for a neighbourhood or an entire city.

CO_2 fluxes can also be estimated via direct measurements using eddy-covariance flux measurements. Historically, the eddy-covariance method was first used in rural environments. It is a well-established method in such environments for which there exist worldwide networks

* Corresponding author.
E-mail address: marine.goret@meteo.fr (M. Goret).

https://doi.org/10.1016/j.aeaoa.2019.100042
Received 12 September 2018; Received in revised form 11 June 2019; Accepted 16 June 2019
Available online 28 June 2019

using standard procedures (Baldocchi et al., 2001). In urban areas, it is a newer method; however, the number of eddy-covariance flux measurements has grown rapidly during the last 20 years (Vogt et al., 2006; Björkegren and Grimmond, 2018; Stagakis et al., 2019). CO_2 fluxes measured via eddy covariance are representative of the neighbourhood scale. Eddy-covariance and inventory methods usually show good agreement in their estimated CO_2 fluxes (Björkegren and Grimmond, 2018).

The eddy-covariance method allows investigations of the daily cycle of CO_2 fluxes, which is not possible with inventory methods. Such investigations highlight the predominance of human activities when explaining the daily cycle of CO_2 fluxes in urban areas, for example, there are large differences between weekdays and weekends (Järvi et al., 2012; Velasco et al., 2014; Björkegren and Grimmond, 2018). Further, the daily cycle in an urban area is substantially different from that in a rural area. In rural areas, CO_2 assimilation by vegetation leads to negative fluxes around midday, whereas in urban areas, the flux remains positive most of the time because the vegetative uptake is outweighed by anthropogenic CO_2 emissions (Kordowski and Kuttler, 2010; Crawford et al., 2015).

Using the eddy-covariance method, it is possible to measure CO_2 fluxes with a high spatiotemporal resolution; however, unlike inventory methods, the decomposition of the total flux per source and sink remains unknown. Eddy-covariance measurements can be combined with inverse modelling to estimate the decomposition and identify the importance of the different contributors to the total flux and their temporal variability. Nemitz et al. (2002) and Liu et al. (2012) highlighted the importance of traffic. In mid-latitude cities, the contribution from buildings can also be very large due to space heating (Moriwaki and Kanda, 2004; Vesala et al., 2008a; Kordowski and Kuttler, 2010), inducing a large seasonal variability in the CO_2 fluxes. The significance of buildings is highly dependant on the climatology; in tropical and subtropical cities (Weissert et al., 2016; Roth et al., 2017) as well as in some Mediterranean cities (Stagakis et al., 2019), the contribution from buildings is low and the seasonal variability is very low. The importance of urban vegetation for CO_2 fluxes strongly depends on the vegetation plan area density and characteristics. Human respiration also contributes to urban CO_2 fluxes. This is usually calculated from the night-time population density and the mean respiration rate per person (Moriwaki and Kanda, 2004). This approach does not consider the spatiotemporal fluctuation of people between night and day.

To summarise, inventory methods are reputed to estimate the CO_2 fluxes; however, the quality and the spatiotemporal resolution of the evaluation depends on those of the baseline data. Direct measurements of CO_2 fluxes with a high temporal resolution are possible with eddy-covariance methods. Inverse modelling combined with eddy-covariance measurements allows a better understanding of the CO_2 fluxes over urban areas and the ability to identify the main sources and sinks. However, the installation of eddy-covariance systems and their long-term maintenance are expensive and the results are only representative of the neighbourhood scale. In this context, modelling is a promising opportunity to estimate CO_2 fluxes at different time scales (e.g. hourly, daily, monthly and annually) and spatial scales (e.g. neighbourhood and city) at a lower cost.

The present study proposes to include the modelling of sources and sinks of CO_2 (i.e. buildings, traffic, urban vegetation and human respiration) in the urban canopy model Town Energy Balance (TEB) (Masson, 2000). Two factors are identified to explain CO_2 flux variability in urban areas: the variability of human activities and the meteorological conditions. The former is taken into account via schedules of the traffic, human respiration and building contributions. The link between the urban microclimate and the CO_2 fluxes is explicitly modelled using actual meteorological conditions. Building emissions are calculated using the Building Energy Model (BEM) included in TEB, and urban vegetation emissions and uptakes are modelled via the Interactions between Soil, Biosphere and Atmosphere (ISBA) model. Both ISBA and BEM consider the prevailing meteorological conditions in the urban canyon, as modelled by the TEB meteorological observations above the rooftop level.

Very few studies have investigated CO_2 fluxes using a modelling approach. Soegaard and Møller-Jensen (2003) proposed a model for vegetation; however, other contributors to CO_2 fluxes are estimated via inverse modelling. Christen et al. (2011) gathered four independent sub-models to obtain a complete modelling of the CO_2 fluxes. Climatic conditions were considered by the building sub-model but only at a monthly resolution; conversely, we use meteorological data with a 5-min time step. Respiration modelling requires soil temperatures and soil volumetric content observations that, in our approach, are modelled via ISBA. At an annual and monthly scale, the Christen et al. (2011) model is in good agreement with CO_2 fluxes measured using the eddy-covariance method. To our knowledge, our study is the first to propose a modelling of the CO_2 fluxes that fully captures the link between the urban microclimate and the CO_2 fluxes.

In the following, Section 2 presents the CO_2 flux modelling strategy we adopted and developed. Section 3 introduces the measurements used for the model evaluation and the way that they have been processed and exploited. The model results are discussed in Section 4, and conclusions are drawn in Section 5.

2. Implementation of CO_2 fluxes in Town Energy Balance (TEB)

TEB is a surface energy balance model that is able to describe surface–atmosphere interactions in urban areas at a horizontal resolution of 100 m to a few kilometres. The urban surface is described by a representative street canyon, and the energy budget is solved on the different urban facets (i.e. walls, roof, road and urban vegetation). TEB is forced using meteorological data representative of the air above the roof level. It is part of SURFEX (SURFace EXTernalisée in French) (Masson et al., 2013), a surface model that simulates surface–atmosphere interactions for different types of surfaces (i.e. urban areas, natural land covers, rivers and lakes, and oceans).

The reference version of TEB used here is described by Schoetter et al. (2017) and is an improved version of the model implemented in SURFEX-v7.3. It includes a modelling of the building energy demand by BEM (Bueno et al., 2012; Pigeon et al., 2014) with a parameterisation of a variety of human behaviours introduced by Schoetter et al. (2017). The urban vegetation is described by the ISBA model (Noilhan and Planton, 1989). The ISBA model is forced by the meteorological conditions inside the street canyons simulated by TEB following the approach of Lemonsu et al. (2012).

In the following subsections, we detail our strategy to model the CO_2 fluxes in TEB for the main sources and sinks of CO_2, which are buildings, urban vegetation, traffic and human respiration. The contributions from buildings and urban vegetation are modelled in detail because they depend on the prevailing meteorological conditions. Our modelling approach allows the impacts of the urban climate on the CO_2 fluxes due to buildings and urban vegetation to be considered. The models of traffic and human respiration are simpler because these contributions only slightly depend on the meteorological conditions.

2.1. Buildings

CO_2 fluxes due to buildings are a consequence of the energy consumption in the buildings. The relationship between the energy consumption and the CO_2 fluxes depends on the energy source. We adopt the following general modelling strategy: first, we calculate the energy consumption for each source of energy (SOE), and then we convert this energy into a CO_2 flux.

Four sources of energy are defined in the model:

- sources that do not eject any CO_2 or water vapour locally (electricity and urban heating networks), hereafter referred to as ELEC;

- gas, hereafter referred to as GAS;
- fuel oil, hereafter referred to as FUEL; and
- other sources (mainly wood), hereafter referred to as OTHER.

Energy consumption and CO_2 fluxes are linked by emission factors that represent the mass of the CO_2 emitted locally per Joule of consumed energy. Default values of the emission factors depending on the SOE are given in Table 1.

The energy consumption is estimated by BEM, which is included in TEB. It calculates the energy consumed for space heating and air conditioning as a function of the prevailing meteorological conditions, the characteristics of the building envelope (e.g. the presence of insulation materials) and the building use and human behaviour (e.g. the temperature setpoint for heating). The BEM also takes into account heat release due to cooking, electrical appliances and lighting.

We improved the BEM by adding a representation of the energy use for domestic warm water in order to calculate the related CO_2 emissions. For the sake of simplicity, we assumed that there is no heat exchange between buildings and domestic warm water. The energy demand for domestic warm water per square meter needs to be specified by the user, the default BEM value is zero. The need for energy for warm water decreases during the night, with the same modulation as the internal heat release due to cooking and electrical appliances.

The total CO_2 fluxes due to buildings (F_{CO_2bld}) is modelled as the sum of the contributions from heating (F_{CO_2heat}) and domestic warm water (F_{CO_2hw}):

$$F_{CO_2bld} = F_{CO_2heat} + F_{CO_2hw}. \quad (1)$$

Air conditioning is not considered because we assume that it is entirely electric. Building energy demands not related to heating, ventilation and air conditioning (non-HVAC) are also assumed to be entirely electric. This leads to a slight underestimation of the CO_2 fluxes because cooking appliances may use gas or fuel instead of electricity. This approximation is acceptable because the energy consumption due to cooking is usually small compared to heating energy consumption (less than 10% in France[1]). However, this value is only valid in France and could vary for countries with different climates (Velasco et al., 2013) or socio-economic contexts.

Fractions of buildings heated by a given source of energy (f_{SOE}) are introduced as new input parameters in TEB for the modelling of CO_2 fluxes due to heating. f_{SOE} are relative to the energy demand and not the energy consumed. The efficiency of the heating system (η_{SOE}) is used to relate the energy demand and the energy consumption:

$$F_{CO_2heat} = Q_{heat} * \left(\sum_{SOE} f_{SOE} * \frac{EF_{SOE}}{\eta_{SOE}} \right), \quad (2)$$

where Q_{heat} is the energy demand for heating per square meter of building.

The main sources of energy for domestic warm water are gas and electricity. The fraction of water heated by gas can be provided to TEB by the user; the default value is set to zero. We assume that the remaining part is heated via electricity:

$$F_{CO_2hw} = Q_{hw} * N_{floor} * \left(f_{HW\_GAS} * \frac{EF_{GAS}}{\eta_{GAS}} + (1 - f_{HW\_GAS}) * \frac{EF_{ELEC}}{\eta_{ELEC}} \right), \quad (3)$$

where Q_{hw} is the energy demand for domestic warm water per square meter of floor. The efficiencies are assumed to be the same for heating systems and water heaters.

We also introduced a calculation of the latent heat emissions due to space heating in the buildings. Details are given in Appendix A.

[1] Données statistiques du CEREN 2015 [2015 Statistical data from CEREN].

Table 1
Characteristics of heating systems by source of energy. The values for the emission factors are taken from ADEME (the French Agency for Environment and Energy Management) (Chêne-Pezot, 2005). The efficiency is defined as the ratio between the useful energy and the total available energy (sensible heat and latent heat). HHV/LHV is the ratio between the Higher Heating Value and the Lower Heating Value (see Appendix A). It matches the ratio between the total quantity of energy (latent and sensible) and the quantity of sensible energy contained in a source of energy.

Source of energy (SOE)	Emission factor ($kgCO_2/J$) (EF)	Efficiency (η)	HHV/LHV
ELEC	0	1.0	1.00
FUEL	5.7×10^{-8}	0.7	1.11
GAS	7.5×10^{-8}	0.7	1.07
OTHER	9.2×10^{-8}	0.7	1.11

2.2. Vegetation

We use the approach introduced by Lemonsu et al. (2012) to describe the in-canyon urban vegetation. The ISBA model (Noilhan and Planton, 1989) is called from within TEB, which means that the interactions between the meteorological conditions in the street canyon and the urban vegetation are explicitly taken into account. The soil is described using the multilayer diffusion scheme of ISBA (Boone et al., 2000; Decharme et al., 2011). The ISBA model follows a big leaf approach. We distinguish three patches: bare ground, low vegetation and high vegetation. Several vegetation types are available for each patch. The vegetative characteristics are adjusted as a function of the vegetation type.

The daily cycles of the carbon and water vapour fluxes between the vegetation and the air in the street canyon are simulated using the CO_2 responsive A-gs version of ISBA (Calvet et al., 1998, 2004). The CO_2 fluxes are calculated as the difference between assimilation due to photosynthesis and release due to respiration.

Photosynthesis constitutes the net CO_2 assimilation of the canopy. CO_2 assimilation is first estimated at the leaf level. The assimilation depends on the CO_2 concentration in the prevailing air, the skin temperature of the plant and the photosynthetically active radiation (PAR). No distinction between direct and diffuse radiation is made here; the PAR at the top of the vegetation canopy is derived from the incident down-welling solar radiation with a constant factor of 0.48. The influence of droughts is taken into account via different modelling strategies depending on the vegetation height (low or high vegetation) and the way the vegetation deals with moisture stress (drought avoiding or drought tolerant) (Calvet, 2000; Calvet et al., 2004). The net assimilation of the vegetation canopy (photosynthesis) is calculated by integrating the net CO_2 assimilation at the leaf level using a three-point Gauss quadrature method. For this integration, we assume that the vertical distribution of leaves is homogeneous and that wet leaves (after rainfall) do not assimilate CO_2.

The ecosystem respiration R_e is calculated using a Q_{10} model based on Van't Hoff's equation, with a reference temperature of 25°C:

$$R_e = Re_{25} * f(w_g) * Q_{10}^{(T_{soil}-25)/10}. \quad (4)$$

Here, Q_{10} is set to 2.0. T_{soil} is the temperature in degrees Celsius of the root-zone soil layer. Re_{25}, the reference respiration rate of the ecosystem at 25°C, needs to be specified by the user. $f(w_g)$ is a scale factor that takes into account the effect of the soil moisture (Albergel et al., 2010). It is calculated as

$$f(w_g) = min(1, w_g/w_{fc}), \quad (5)$$

where w_g is the soil moisture and w_{fc} is the soil moisture at field capacity.

The leaf area index evolves during the simulation depending on the biomass evolution due to the photosynthetic activity (Calvet and Soussana, 2001). Three biomass pools are considered: the leaf biomass,

the active structural biomass and the below ground structural biomass. The effects of nitrogen dilution are taken into account.

2.3. Traffic

The CO_2 fluxes due to traffic are modelled using a simpler approach than the CO_2 fluxes due to buildings and urban vegetation because we assume that the meteorological conditions are not a key factor in explaining the spatiotemporal variability of traffic.

The user needs to provide the annual mean value of the CO_2 fluxes due to traffic for each grid mesh; this value is modulated as a function of the hour of the day, the day of the week and the month of the year (Equation (6)).

$$F_{CO_2 tr}(m, d, h) = \overline{F_{CO_2 tr}} * M_{tr}^{y}(m) * M_{tr}^{w}(d) * M_{tr}^{d}(h) \quad (6)$$

Here, $F_{CO_2 tr}$ denotes the CO_2 flux due to traffic, $\overline{F_{CO_2 tr}}$ is its annual mean value and $M_{tr}^{y}(m)$, $M_{tr}^{w}(d)$ and $M_{tr}^{d}(h)$ are the modulation factors as a function of the month of the year, the day of the week and the hour of the day, respectively.

By default, the modulation is based on the solar time; however, it can be expressed as a function of the legal time if the latter is provided. There are default values for the modulation factors; however, we advise users to provide site-specific values to represent a spatiotemporal variability of the traffic-related CO_2 flux that is as detailed as possible.

We modified the existing approach for the calculation of the sensible and latent heat fluxes due to traffic to be more consistent. It is now similar to the approach followed for the CO_2 fluxes.

2.4. Human respiration

Human respiration can be an important source of CO_2 in urban areas. Moriwaki and Kanda (2004) reported that, in one residential area of Tokyo, human respiration accounted for 38% of the total CO_2 flux in summer and 17% of the total in winter.

The amount of CO_2 exhaled by one person depends on the person's activity level and physical characteristics. Here, we take the population average value of the CO_2 emission rate given by Moriwaki and Kanda (2004), which is 8.87×10^{-6} CO_2 kg/s/person. This average emission rate is multiplied by the population density to obtain the total CO_2 flux due to human respiration. The population density can be modulated depending on the hour of the day, the day of the week and the month of the year, as in the case of traffic. The CO_2 flux due to human respiration ($F_{CO_2 hr}$) is expressed as

$$F_{CO_2 hr}(m, d, h) = \overline{P_{dens}} * M_{hr}^{y}(m) * M_{hr}^{w}(d) * M_{hr}^{d}(h) * E_{hr}^{CO_2}, \quad (7)$$

where $\overline{P_{dens}}$ indicates the average population density and $M_{hr}^{y}(m)$, $M_{hr}^{w}(d)$ and $M_{hr}^{d}(h)$ indicate the modulation factors as a function of the month of the year, the day of the week and the hour of the day, respectively.

3. The CAPITOUL campaign

The Canopy and Aerosol Particle Interactions in the Toulouse Urban Layer (CAPITOUL) campaign took place in Toulouse between February 2004 and February 2005. Toulouse is located in the southwest of France. It is influenced by both the Atlantic Ocean (230 km to the west) and the Mediterranean Sea (150 km to the southeast). The Pyrenees Mountains are located 80 km south of Toulouse. Winters are mild, and summers hot and dry. Here, we focus on measurements taken in the city centre of Toulouse, at the Monoprix site. Details concerning the campaign and its instrumentation can be found in Masson et al. (2008). Fig. 1 shows an aerial view of the site. The neighbourhood matches LCZ 2 (Stewart and Oke, 2012) with primarily 4–5 storey brick buildings and little vegetation. We first describe the CO_2 flux measurements in detail (data processing, representativeness and uncertainties) and then the dataset used for the model evaluation.

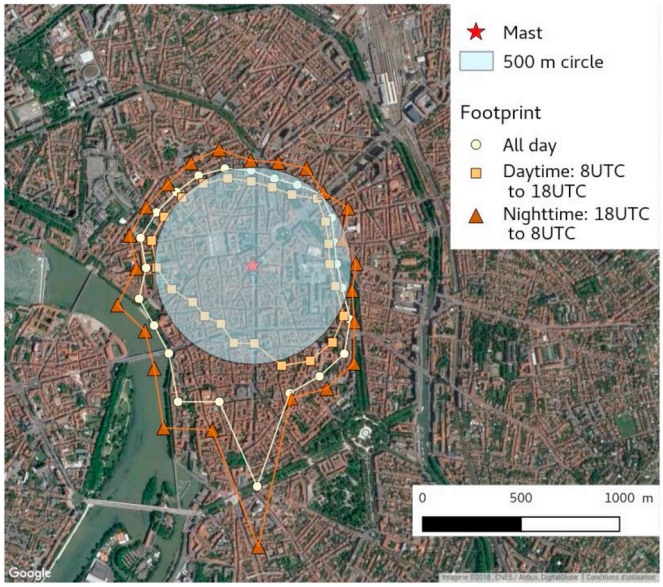

Fig. 1. Mean 80% fetch per direction (15° bins) for the CO_2 fluxes measured on the mast.

3.1. CO_2 flux measurements

3.1.1. Data processing

The CO_2 fluxes were measured using the eddy-covariance technique. An open-path LICOR-7500 combined with a GILL sonic anemometer measured the fluxes at the top of a pneumatic tower installed on the roof of a 20-m-high building (the Monoprix site). The eddy-covariance measurement device was located 48.05 m above ground level and was lowered to 38.23 m during strong wind events (Appendix D).

For the purpose of this study, several corrections were applied to the raw measurement data. Air density fluctuations were taken into account via the Webb correction (Webb et al., 1980). Isolated peak values of the wind speed and the CO_2 concentration were removed. A peak value is characterised by a difference between the actual value and the average of the previous and next values of more than 30 m s^{-1} (at 50 Hz) for the wind speed and 28 ppm (at 20 Hz) for the CO_2 concentration. We also used a spike removal algorithm. The moving average and moving standard deviations were calculated with time intervals of 200 s for the wind speed and 60 s for the CO_2 concentration. Measurements were removed if the deviation from the mean was greater than seven standard deviations for the wind and four standard deviations for the CO_2 concentration. The lag between the anemometer and the LICOR was corrected. A high-pass filter with a cutoff frequency of 0.0008 Hz was applied to remove the long-term CO_2 concentration fluctuations. Observations made during rainy periods were removed depending on the strength of the signal received by the LICOR. The standard 2D rotation was applied. The main impact of this rotation is in the winter; it increases the average CO_2 flux by 1.8 μmol m^{-2} s^{-1}, which represents only a 4% increase in the flux compared to that without the rotation correction. Two quality flags proposed by Foken et al. (2004) were calculated. One quality flag quantifies the stationary component of the turbulence; the other quantifies its intensity. Only the former was used because the validity of the second is questionable in urban environments because it is based on parameterizations derived for areas with low canopy heights (Thomas and Foken, 2002). The quality flag quantifying the stationary component of the turbulence compares the average CO_2 flux for a 30-min period with the averages for short 5-min intervals within this period. In this study, we only analysed data with a quality flag equal to or lower than five, which

means that the observations are of medium to very good quality and are usable for statistical analyses. Finally, a threshold on the friction velocity ($0.15\,m\,s^{-1}$) was applied to remove periods with insufficient turbulence.

After all the corrections were applied, the data availability reached at least 51% for each season (Appendix B). We chose not to fill gaps in the time series because our goal was to compare the measured and modelled CO_2 fluxes. This comparison is based on instants when observations were available.

3.1.2. Data representativeness

We performed a footprint analysis to obtain the area represented by the CO_2 fluxes measured on the mast. Several types of footprint models are available (Vesala et al., 2008b). The easiest models are analytical ones; however, such models are not appropriate for a terrain as complex as a city. We used the Flux Footprint Predictions (FFP) model of Kljun et al. (2015), which is a parameterization based on the backward Lagrangian stochastic particle dispersion model LPDM-B (Kljun et al., 2002). This model was selected because the roughness length value for the simulated area is in the range of the values tested in the simulations that were performed to build the model. The advice of Kljun et al. (2015) to use the FFP model above the roughness sublayer and below the entrainment layer was followed because the eddy-covariance measurements were made in the inertial sublayer (Appendix D). We invalidated the footprint values when the observations did not fulfil the atmospheric stability condition proposed by Kljun et al. (2015): $-15.5 < z_m/L$, where z_m is the measurement height. With this criterion, a value for the footprint could be obtained for more than 99% of the CO_2 flux measurements.

The footprint model was applied each half hour. This implicitly assumes that the footprint is constant during each 30-min measurement period. The required parameters for the FFP model are defined as follows.

- The mean building height (z_H) is 15 m. This was calculated by Pigeon et al. (2008) based on administrative data of the building outlines and heights.
- Following Grimmond and Oke (1999), we set the aerodynamic roughness length (z_0) to 10% of z_H and the zero-plane displacement length (z_d) to 70% of z_H.
- The measurement height z_m was set equal to the receptor height minus z_d.
- No measurements of the boundary layer height were available. For stable and neutral conditions, we used the formula of Nieuwstadt (1981) as proposed by Kljun et al. (2015). For unstable conditions, the fetch is not very sensitive to the boundary layer height. We therefore assumed a boundary layer height of 250 m during the night (from 20 UTC to 6 UTC) and of 1000 m during the day (from 6 UTC to 20 UTC).

Mathematically, a footprint tends to infinity. Here, we define the fetch as the minimum radius of a circle centred on the mast such that at least 80% of the CO_2 that reaches the mast is emitted within this circle. The FFP model calculates a two-dimensional footprint with an along-wind distribution and a crosswind distribution. We used only the along-wind repartition to calculate the fetch for each half hour.

The 30-min periods were split into 24 classes according to the mean wind direction (bins of 15°). The average long-term fetch was then calculated for each wind direction class. The mean fetch was approximately 500 m for each class (Fig. 1). It was slightly larger for periods with a southerly wind direction; however, such periods are quite rare. Because the urban morphology is homogeneous in the vicinity of the mast, we assumed that the CO_2 fluxes measured at the mast were representative of the fluxes in a 500-m-radius circle centred on the mast.

3.1.3. Storage of CO_2 below the measurement height

Storage of CO_2 in the air column below the height of the eddy-covariance measurements leads to uncertainties in the temporal behaviour of the CO_2 emissions. Crawford et al. (2015) demonstrated that, in Vancouver during the night, the CO_2 concentration is 50 ppm higher at street level than 50 m above street level. The accumulation of CO_2 in the street canyon during the night leads to underestimations of emissions by tower measurements during the late evening and night and overestimations in the morning.

Storage below the mast observation level is quantified using the half-hourly CO_2 concentration observations at the mast and rooftop levels. Bjorkegren et al. (2015) showed that these two measurement heights are sufficient to quantify the CO_2 storage. More details concerning the storage calculation method are given in Appendix E.

The average storage is minimal in the afternoon and increases during the night, and maximal values occur around 7 UTC. At this time, the mean CO_2 storage flux is approximately $3\,\mu mol\,m^{-2}\,s^{-1}$ and the 90th percentile is approximately $8\,\mu mol\,m^{-2}\,s^{-1}$. In percentage terms, the mean storage is maximal at 1 UTC when the storage is largest and the fluxes are smallest; at this time, it reaches 13% of the flux. CO_2 storage then decreases until 15 UTC when it accounts for less than 4% of the CO_2 flux. These percentages are very small compared to what has been reported for rural sites (Yang et al., 2007). This can be explained by the fact that the nocturnal boundary layer usually becomes stable in rural areas, whereas it remains neutral or slightly unstable in urban areas.

As suggested by Crawford et al. (2011), to avoid double counting the storage flux, no corrections of the measurements for the CO_2 storage were made. Instead, we chose to plot the mean absolute storage flux in the graphs in the evaluation section to provide an evaluation of the errors due to the storage phenomenon.

3.2. Input data for the TEB simulation

The goal of the TEB simulation is to simulate CO_2 fluxes comparable to the measured fluxes. Based on the results of the footprint analysis (Section 3.1.2), we simulated a 500-m-radius circle centred on the mast. This area was represented by a single grid mesh because we know that the urban morphology is relatively homogeneous in this area (Pigeon et al., 2008).

The meteorological forcing parameters required by TEB are listed in Table 2. Nearly all the parameters were measured each minute at the mast. Hourly means of the meteorological parameters were calculated to obtain the forcing data for TEB. Data gaps were filled by observations from a meteorological station operated by Météo-France located 6.5 km west-southwest of the mast (the Météopole station). The temperature and relative humidity from the Météopole station were corrected with the mean difference between the Météopole station and the mast. Mean differences were calculated for each hour of the day. The cloud cover measured at the Blagnac airport (7 km northeast of the mast) was used to separate the direct from the scattered downward short-wave radiation. Linear interpolation was used to complete the cloud cover and CO_2 concentration time series. All precipitation was assumed to be liquid (snow is very rare in Toulouse). The wind speed was measured at different heights depending on the weather conditions because the mast was lowered for safety reasons when high wind speeds were forecast. The wind speed measured at the lowest positions of the mast were corrected to the reference level (the highest position) assuming a logarithmic wind profile:

$$u(z_{rec}) = \frac{u_*}{\kappa} ln\left(\frac{z_{rec} - z_d}{z_0}\right), \tag{8}$$

where u is the wind speed, z_{rec} is the receptor height, u_* is the friction velocity, κ is the von Kármán constant, z_d is the zero plane displacement height and z_0 is the roughness length. See Section 3.1.2 for more details

Table 2
Meteorological forcing data for the TEB model. The Blagnac airport is located 7 km to the northeast of the mast. The Météopole station is located 6.5 km to the west-southwest of the mast and is operated by Météo-France.

Model forcing parameter	Observed parameter	Main source	Fill in source/ method	Data processing
Pressure (Pa)	Pressure	Mast	Météopole and Blagnac	–
Air temperature (°C)	Air temperature	Mast	Météopole with correction	–
Specific humidity ($kg\,kg^{-1}$)	Relative humidity	Mast	Météopole with correction	–
Direct downward short-wave radiation ($W\,m^{-2}$)	Downward short-wave radiation	Mast	Météopole	Direct/scattered separation depending on cloud cover
	Cloud cover	Blagnac	Linear interpolation	
Scattered downward short-wave radiation ($W\,m^{-2}$)	Downward short-wave radiation	Mast	Météopole	Direct/scattered separation depending on cloud cover
	Cloud cover	Blagnac	Linear interpolation	
Downward long-wave radiation ($W\,m^{-2}$)	Downward long-wave radiation	Mast	Météopole	–
CO_2 concentration ($kg\,m^{-3}$)	CO_2 concentration	Mast	Linear interpolation	–
Rain rate ($kg\,m^{-2}\,s^{-1}$)	Rain rate	Mast	Météopole	–
Snow rate ($kg\,m^{-2}\,s^{-1}$)	–	–	–	Precipitation is assumed to be liquid
Wind speed ($m\,s^{-1}$)	Wind speed	Mast	Météopole	Height correction assuming a logarithmic wind profile
Wind direction (degrees from North, clockwise)	Wind direction	Mast	Météopole	–

concerning z_d and z_0.

By division, we obtain

$$u(z_{ref}) = u(z_{rec})^* \frac{ln\left(\frac{z_{ref}-z_d}{z_0}\right)}{ln\left(\frac{z_{rec}-z_d}{z_0}\right)}, \quad (9)$$

where z_{ref} is the reference level.

The main site characteristics are listed in Table 3. The most relevant parameters for the CO_2 flux calculation are given in Table 4.

In the study area, most buildings are historical (pre-WWII) mid-rise red brick buildings with tiled roofs (Table F.7) originally for residential use. Many buildings have been converted at least partially into offices, commercial establishments and restaurants. To represent this variety of building uses, we employed the method proposed by Schoetter et al. (2017), who distinguished a non-heated fraction, a commercial fraction, an office fraction and three residential fractions with different heating setpoints. The fractions of the non-residential building uses are given in Table 4. The fractions of the residential uses with different heating setpoints were derived from the energy control behaviour (ECR) (see Schoetter et al. (2017) for more details, ECR is referred to as ET in this earlier study). The ECR, defined by Bourgeois et al. (2017), combines information on the heating system type (collective or individual), the source of energy for space heating and the age of the inhabitants.

Various parameters are required for each fractional building use, e.g. daily schedules for building occupation, the temperature setpoint, the non-HVAC internal heat release, the use of ventilation and shading. We used the values proposed by Schoetter et al. (2017). In Schoetter et al. (2017), the non-HVAC internal heat release in residential buildings was specified depending on the Equipment-Intensity-of-Use indicator (defined by Bourgeois et al. (2017)). This indicator depends on the number of inhabitants per habitable floor area, the space heating system type (collective/individual) and the heating source. Its values for the area of investigation are given in Table 4. For the residential use, we set the energy consumed for domestic warm water to 25% of the

Table 3
Main site characteristics.

Parameter	Value
Building plan area density (λ_p)[a]	0.62
Road plan area density (λ_r)[a]	0.28
Vegetation plan area density (λ_v)[a]	0.10
Facade surface density[a,b]	1
Building height (z_H)[c]	15 m
Roughness length for the momentum (z_0)	1.5 m

[a] Bocher et al. (2018): mapuce.orbigis.org.
[b] Total facade area surface divided by the total horizontal urban surface.
[c] Pigeon et al. (2008).

Table 4
Relevant parameters for the CO_2 flux calculation.

Buildings	
Fraction of electrical heating[a] (f_{ELEC})	0.6
Fraction of gas heating[a] (f_{GAS})	0.39
Fraction of fuel heating[a] (f_{FUEL})	0.01
Fraction of households using gas for domestic warm water[a] (f_{HW_GAS})	0.5
Fraction of collective housing[b]	0.25
Fraction of commercial building use[b]	0.10
Fraction of office and educational building use[b]	0.55
Fraction of non-heated buildings[b]	0.10
Fraction of households with high energy control behaviour (ECR)[c]	0.60
Fraction of households with low ECR[c]	0.40
Fraction of households with high Equipment-Intensity-of-Use[c]	0.24
Fraction of households with medium Equipment-Intensity-of-Use[c]	0.70
Fraction of households with low Equipment-Intensity-of-Use[c]	0.06
Vegetation	
Leaf area index (high vegetation)	3.5
Respiration rate of the ecosystem at 25°C (Re_{25})	$2.2 \times 10^{-7}\,kg\,m^{-2}\,s^{-1}$
Traffic	
Mean annual CO_2 flux	$5.6 \times 10^{-7}\,kg\,m^{-2}\,s^{-1}$
Mean emission factors of CO_2[d]	$0.47\,kg\,km^{-1}$
Human respiration	
Population density[e]	$13{,}000\,hab\,km^{-2}$

[a] 2011 census of the French population by the French National Institute on Economics and Statistics (INSEE) https://www.insee.fr/fr/statistiques/2028584a.
[b] Estimated by combining information on the building type, urban morphology and population density (Bocher et al., 2018). The methodology is described in Schoetter et al. (2017).
[c] These indicators have been defined by Bourgeois et al. (2017). They use the ENERGIHAB survey on human behaviour in the Île-de-France region to calibrate statistical models that allow the prediction of indicators based on the French national census.
[d] Derived from Hugrel and Joumard (2006).
[e] Bocher et al. (2018): mapuce.orbigis.org.

Table 5
Description of the different model configurations used in the sensitivity experiment.

Configuration	Description/Modifications	Motivations
DEF	Constant internal building temperature (19°C).	Simple parameterization
REAL_BEHA	Use of fractional building use and behaviour with default values. (Schoetter et al., 2017)	–
INT_MASS	Representation of intermediary floors by a 20-cm-thick concrete layer and a 3-cm-thick wood layer.	Intermediary floors are represented by a 3-cm-thick layer of wood in the architectural database, which might lead to an underestimation of the heat storage capacity of the building and, as a consequence, deteriorate the simulated daily cycle of the heating energy consumption.
TEMPE	In residential buildings, the heating setpoint temperature is reduced by 2°C when the buildings are vacant and during the night. In office, commercial and educational buildings, the heating setpoint temperature is set to 22°C (previously 21°C) when the buildings are occupied during the day and 17.5°C (previously 20°C) otherwise.	The difference in the heating setpoint temperature between night/day and unoccupied/occupied buildings is only 1°C in the configuration proposed by Schoetter et al. (2017). This relatively low difference was retained because no information on the heating setpoint modulation between day and night was available.
OCCUP	The occupation probability of offices between 16 UTC and 19 UTC was increased from 0.25 to 0.7. The occupation probability of commercial establishments between 16 UTC and 19 UTC was increased from 0.8 to 0.9 on weekdays and from 0.75 to 0.95 on Saturdays.	These modified schedules better represent the use and occupation of offices and commercial establishments in the domain of the investigation.
QIN	The non-HVAC internal heat release in commercial, office and educational buildings was reduced from 10 to 15 $W\,m^{-2}$ to 7 $W\,m^{-2}$.	The original value could be realistic for an office with a large number of electrical appliances but is likely too high when an entire building including corridors, halls and meeting rooms is modelled. Lower non-HVAC internal heat releases lead to an increased heating energy demand and, as a consequence, larger CO_2 fluxes during the heating season.

non-HVAC energy consumption. The energy was set to 0% for the other building uses.

The vegetation consists primarily of temperate broad-leaf cold-deciduous summer-green high vegetation (Table F.8). The value of Re_{25} needs to be specified to account for the CO_2 emissions due to respiration by the urban vegetation (Section 2.2). Usually, Re_{25} is determined from the CO_2 fluxes measured at night when photosynthesis does not take place. This method cannot be used in urban areas because sources of CO_2 other than vegetation exist at night. The ratio of the ecosystem respiration to the gross primary production (GPP) over one year is relatively constant from one year to another and equal to 0.71 for French agricultural sites (J.-C. Calvet, personal communication). Using Equation (4), we obtained a value of $2.2 \times 10^{-7}\,kg\,m^{-2}\,s^{-1}$ for Re_{25} with the following relation:

$$Re_{25} = \frac{0.71 * \int_{1year} GPP(t)\,dt}{\int_{1year} f(w_g(t)) * Q_{10}^{(T_{soil}(t)-25)/10}\,dt}. \quad (10)$$

The GPP values were calculated by the ISBA model using a 5-min time step.

The average daily, weekly and annual traffic cycles (Fig. 2) were calculated based on traffic count data taken during the campaign near the mast for two different roads: Rue d'Alsace-Lorraine and Rue de Lafayette. The daily, weekly and annual cycles for these two roads are very similar; therefore, we averaged them.

In the footprint area of CAPITOUL, vehicles adopt an urban driving style with a speed limit of 50 $km\,h^{-1}$. The fleet is composed of cars (78%), vans (13%), heavy vehicles (6%) and motorcycles (3%). The mean emission factors of CO_2, sensible heat and latent heat for a fleet representative of traffic in Toulouse were derived from the emission factors for French urban traffic per type of vehicle (Hugrel and Joumard, 2006) combined with the distribution of the traffic per type of vehicle observed during the campaign.

We divided the annual average value of the sensible heat flux due to traffic given by Pigeon (2007) for the centre of Toulouse (8 $W\,m^{-2}$) by the average emission factor for sensible heat to obtain an estimate of the number of kilometres travelled. The CO_2 and latent heat emissions were then estimated by multiplying the number of kilometres travelled by the respective emission factors (Table F.9).

The population density was assumed to be constant; spatiotemporal variations, for example due to commuting, were neglected. The main reason for neglecting these fluctuations was the difficulty in obtaining a reliable estimate of the population density fluctuation through time for our case study.

The initial conditions for our simulation were taken from a spin-up simulation of 1 year using the above-mentioned forcing from 20 February 2004 to 19 February 2005. This spin-up initialised the biomass reservoirs, temperature in the buildings, soil temperature and soil moisture.

4. Model evaluation for a dense European city centre

4.1. Sensitivity of modelled CO_2 fluxes on parameters related to building use and human behaviour

4.1.1. Adjustment of the parameters and model sensitivity

In this section, we investigate the sensitivity of the modelled CO_2 fluxes to parameters related to building use and human behaviour. Different configurations of BEM are investigated: a default (DEF) configuration, which is the historical configuration of BEM without fractional use and behaviour, and five configurations with fractional use and behaviour. Using fractional use and behaviour requires the adjustment of numerous parameters. We used our knowledge of the modelled area to adjust the default values proposed by Schoetter et al. (2017). We used a step-by-step approach, changing one parameter after another. A new experiment was performed each time to study the influence of each modification. The different model configurations are described in detail in Table 5. We only show results for DJF (December, January and February) because it is the season when, due to the high energy demand for space heating, the CO_2 fluxes due to buildings are the largest.

The default configuration (DEF) is very simple but is unable to reproduce the daily cycle of the CO_2 fluxes well: the model and the observations are in phase opposition (Fig. 3). The CO_2 fluxes are too high during the night and too low during the day. Using the fractional use and behaviour with default values for the parameters (the REAL_BEHA configuration) improves the results during the night; however, the CO_2 fluxes are still overestimated. There is also a minimum in the CO_2 fluxes at midday that is not present in the observations. Increasing the thickness of the intermediary floors with a 20-cm concrete layer (the INT_MASS configuration) slightly lowers the CO_2 fluxes during the night and increases them during the day. This is due to the increased

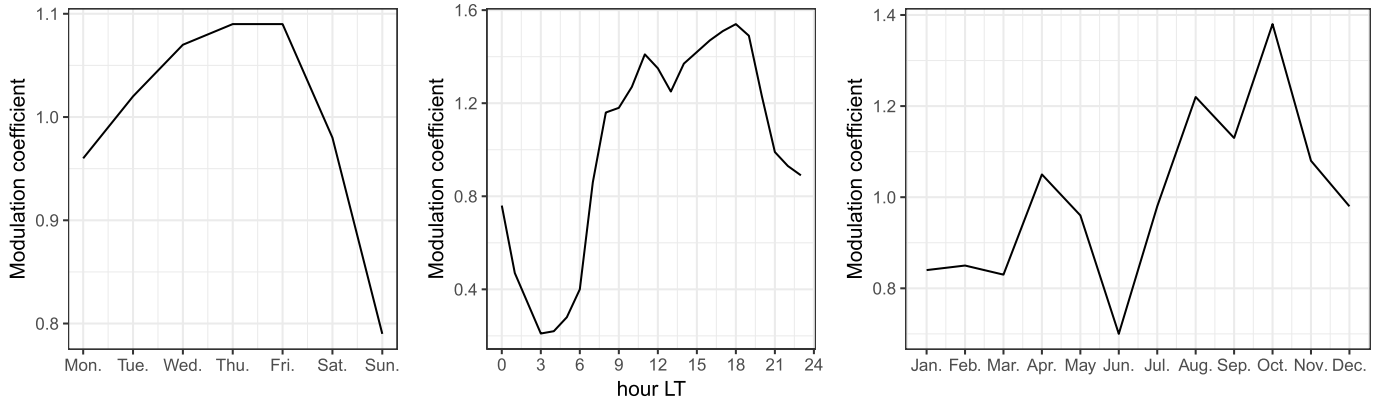

Fig. 2. Daily, hourly and annually modulation coefficients of the traffic emissions. The coefficients were calculated from the traffic count during the CAPITOUL campaign near the measurement mast.

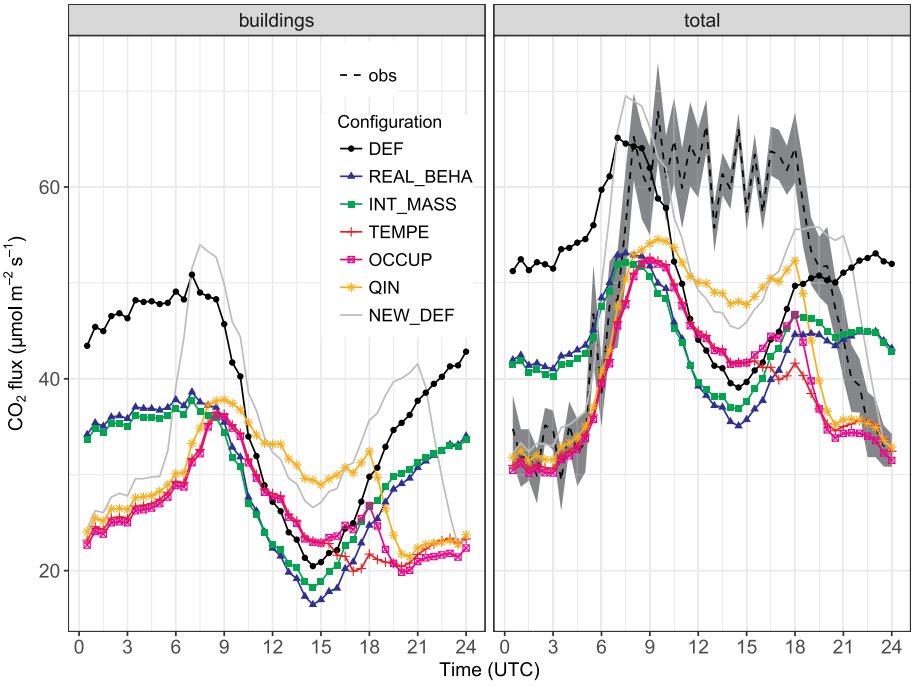

Fig. 3. Daily cycle of the average modelled CO_2 fluxes in DJF for several model configurations: the default model configuration (DEF), a detailed description of the residential behaviour (REAL_BEHA), a larger heat storage capacity of buildings due to thicker intermediary floors (INT_MASS), a change in the heating setpoint temperature (TEMPE), a change in the occupation schedule for offices (OCCUP) and a lower non-NVAC internal heat release in offices (QIN). The experiments are described in detail in Table 5. In the left panel, only the CO_2 fluxes due to buildings are shown. In the right panel, the total CO_2 fluxes are compared to the observations. The grey shading represents the uncertainties in the observations due to CO_2 storage in the air column below the eddy-covariance measurements.

heat storage capacity of the buildings. However, the modification of the CO_2 fluxes due to this change in the building structure is not substantial. Increasing the heating setpoint temperature during the day and decreasing it during the night (the TEMPE configuration) slightly increases the CO_2 fluxes around midday and decreases them during the night. As a result, there is an improvement in the modelled daily cycle of the CO_2 fluxes. A higher occupation of offices between 16 UTC and 19 UTC (the OCCUP configuration) increases the CO_2 fluxes during this time period due to the higher setpoint temperature for space heating. Lowering the non-HVAC heat release inside buildings (the QIN configuration) leads to an increase in the CO_2 fluxes because the heating energy demand increases.

This step-by-step modification of the parameter values shows that CO_2 modelling is strongly sensitive to parameters describing human behaviour: the daily cycle of the CO_2 fluxes due to buildings in the last experiment (QIN) is in phase opposition with the experiment with the default values (REAL_BEHA). Except for the modification of the internal mass, all the modifications (setpoint temperature, occupation probability and internal energy demand) have a clear impact on the CO_2 fluxes. The impacts are immediate: the modification of a parameter for a given period impacts the CO_2 fluxes during this period, for example, a decrease in the night-time setpoint temperature has an effect during the night-time.

The sensitivity analysis shows that the CO_2 fluxes are particularly sensitive to the heating setpoint temperature. We therefore propose a new default setup for the TEB parameters (NEW_DEF) that includes a modulation of the heating setpoint temperature but remains very simple because no fractional building use or human behaviour is considered. This makes it applicable to cities for which these parameters are unknown. The NEW_DEF configuration is similar to the DEF configuration except that the night-time heating setpoint temperature is lowered by 2°C. The daily cycle of the CO_2 fluxes of the NEW_DEF configuration is clearly improved compared to the DEF configuration, and the nocturnal fluxes are close to the observations. The CO_2 fluxes around midday are also closer to the observed values, giving a result comparable to the QIN configuration. In the early morning and late evening, however, the modelled CO_2 fluxes are higher than the observations.

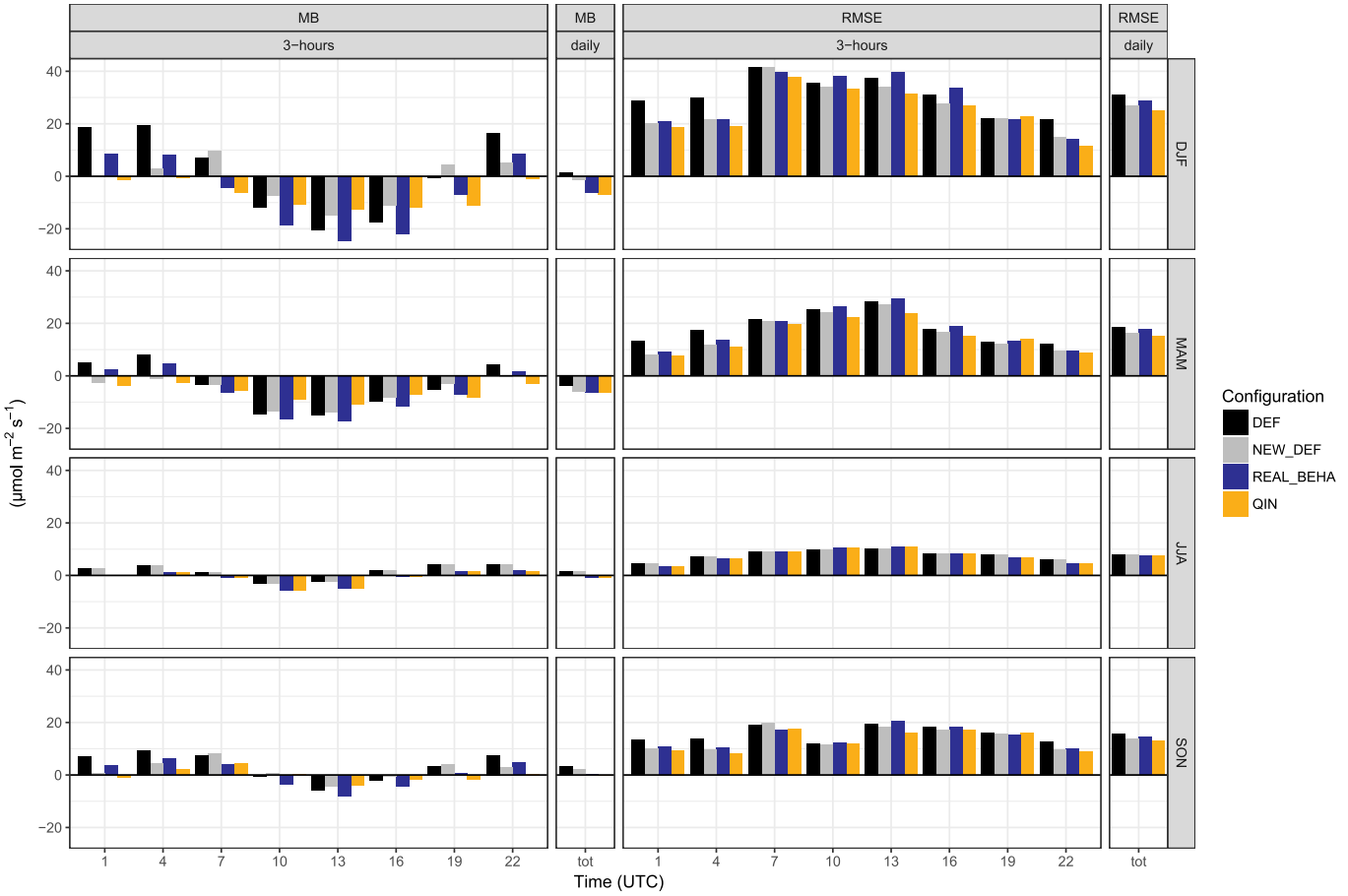

Fig. 4. Mean bias (MB) and root mean square error (RMSE) between the modelled and observed CO_2 fluxes per season for one-year simulations of four model configurations: the historical configuration (DEF), the historical configuration with a decreased setpoint temperature during the night (NEW_DEF), a configuration with fractional building use and behaviour with the default parameter values from Schoetter et al. (2017) (REAL_BEHA) and a configuration with fractional building use and behaviour with adjusted parameter values (QIN). Scores are plotted for each 3-h period as well as for the entire day.

4.1.2. Model statistical scores for the different configurations

We can compare the different model configurations more objectively by calculating statistical scores (mean bias and root mean square error (RMSE)). The comparison is made for the entire year to verify whether the performance of the different experiments in DJF can be generalised to the full year.

The daily average bias for the DEF configuration is low; however, this is a result of the compensation of the negative bias in the afternoon by the positive bias during the night (Fig. 4). The NEW_DEF configuration has a lower bias than the DEF configuration except in MAM (March, April and May). It reproduces the daily cycle of the CO_2 fluxes much better than the DEF configuration. The RMSE is also reduced for the NEW_DEF configuration. The REAL_BEHA configuration performs better (lower RMSE) than the DEF configuration but worse than the NEW_DEF configuration. This result emphasizes that adjustments in the model parameters are essential to fully benefit from the introduction of fractional building use and behaviour. The QIN configuration performs better in terms of the RMSE than any of the other configurations.

The differences between the model configurations are lowest in JJA (June, July and August) because the CO_2 fluxes due to buildings are the smallest in this season. The benefit of a detailed description of building use and behaviour is therefore largest during the heating season.

The NEW_DEF configuration does not perform as well as the QIN configuration; however, it is more robust because it requires less input parameters. Hereafter, the configuration with the fractional building use and behaviour and the adjusted parameters (QIN) will be denoted as the reference configuration (REF).

4.2. Model evaluation for the reference model configuration

The sensitivity study in the previous section highlighted the relevance of model parameters related to building use and human behaviour for the modelled CO_2 fluxes. In this section, we evaluate the results of the REF configuration in detail compared to the observations from the CAPITOUL campaign. We only consider the model output when temporally matching observations are available. In the REF configuration, the parameter values that describe human behaviour have been specifically adjusted for the area of investigation. The results in this section, therefore, quantify the ability of the model to estimate CO_2 fluxes when a large amount of information on the building use and human behaviour is available.

4.2.1. Sensitivity of CO_2 fluxes to footprint variations

Differences between the footprint area for the observations and the modelled area might lead to systematic biases in the model results. We therefore investigated whether the model bias depends on the wind direction and the fetch. Fig. 5 shows that the bias of the CO_2 flux does not depend much on the wind direction. The nocturnal bias for northeasterly wind is slightly smaller in SON (September, October and November) and DJF than that for other wind directions. However, this might not be a robust result due to the small number of observations available for the northeasterly wind direction. An anisotropy in the bias is also found during the day in DJF and to a lesser extent in MAM and SON; however, similar to the nocturnal bias, this is only found for wind directions with few available observations.

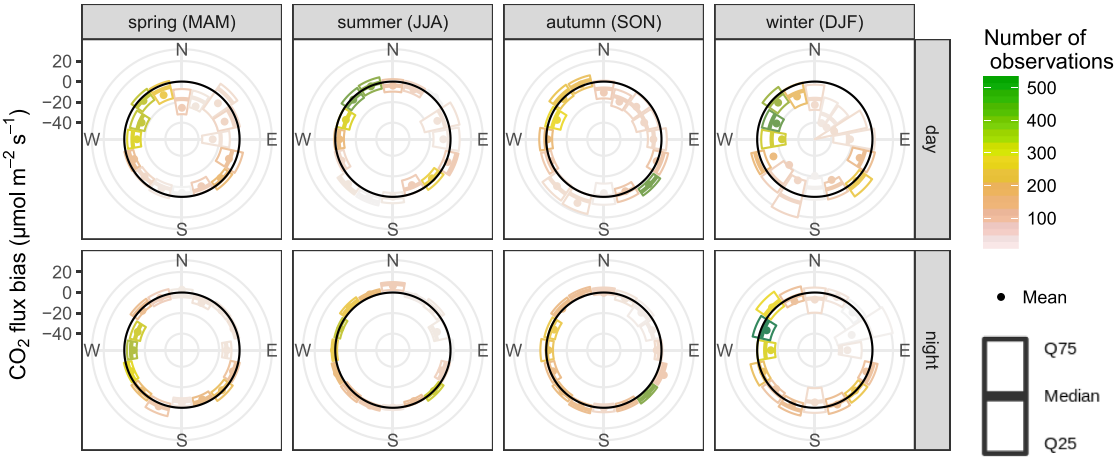

Fig. 5. Seasonal boxplots of the model biases for the CO_2 fluxes per wind direction. Data are split between daytime (from 7 UTC to 19 UTC) on the first line and night-time (from 19 UTC to 7 UTC) on the second line. The black circle indicates no bias.

The model bias (Fig. 6) is not very sensitive to the fetch except when the footprint is very small. This is particularly true in DJF when the model exhibits a larger negative bias during the day and a larger positive bias during the night for periods with a low fetch. In view of these results, we invalidated data when the fetch was in the first decile (a fetch lower than 337 m). The larger negative bias during the day is likely due to chimneys near the measurement mast. For low fetches, their contribution to the total measured CO_2 flux increases and leads to high measured fluxes, which are not representative of the area defined by a circle with a 500-m radius around the mast.

4.2.2. Evaluation of turbulent heat fluxes

Building energy consumption, vegetation and motor traffic influence both the CO_2 fluxes and the turbulent heat fluxes.

Therefore, an evaluation of the turbulent heat fluxes allows a check of whether the adjustment of the BEM parameters that improved the modelled CO_2 fluxes deteriorated the modelled turbulent heat fluxes.

Fig. 7 displays the seasonal average daily cycle of the turbulent latent and sensible heat fluxes. The simulated sensible heat flux agrees well with observations for all seasons. There are larger discrepancies for the latent heat flux. We reduced the maximum surface of the puddles as proposed by Demuzere et al. (2017). This modification improves the results; however, TEB still underestimates the latent heat flux by 5–10 W m^{-2}. No relevant relationship between the latent heat flux bias and the wind speed or time since the last precipitation event was found. The irrigation of urban vegetation and roads could partly explain the negative bias during the day but not during the night. Similar biases have been reported in TEB results by Karsisto et al. (2016) over the Kumpula and Torni sites in Helsinki, Finland. The cause could be missing anthropogenic moisture sources or errors in the eddy-covariance measurements.

4.2.3. Evaluation of CO_2 fluxes

Fig. 8 shows that, for each season, the modelled and observed daily cycles of the CO_2 fluxes agree quite well on weekdays. The daily cycle on Sundays is also captured well. TEB underestimates the daytime CO_2 flux on Saturdays during the heating season. This could be due to the numerous customers visiting commercial establishments, which leads

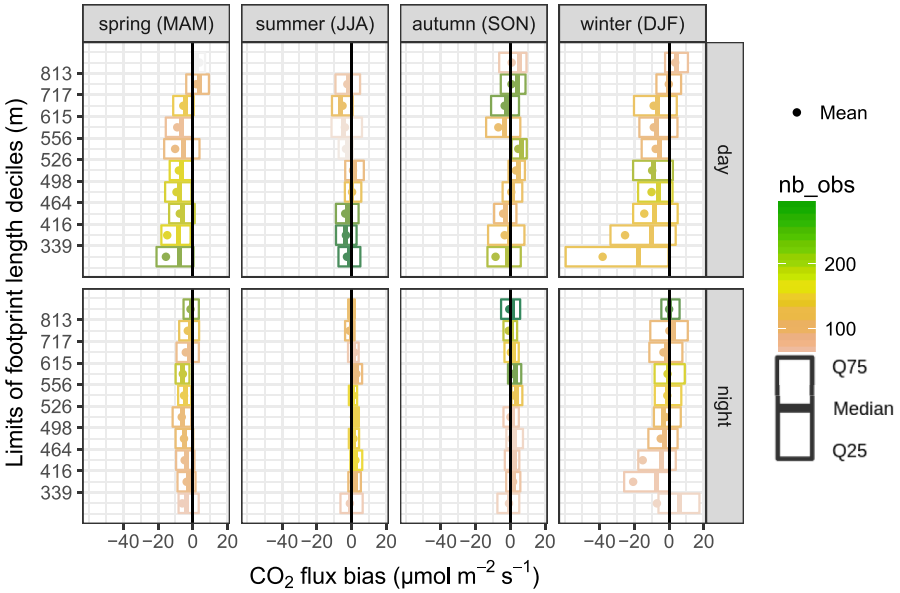

Fig. 6. Seasonal boxplots of the model biases for the CO_2 fluxes per decile of the fetch. Data are split between daytime (from 7 UTC to 19 UTC) on the first line and night-time (from 19 UTC to 7 UTC) on the second line. The black line indicates no bias.

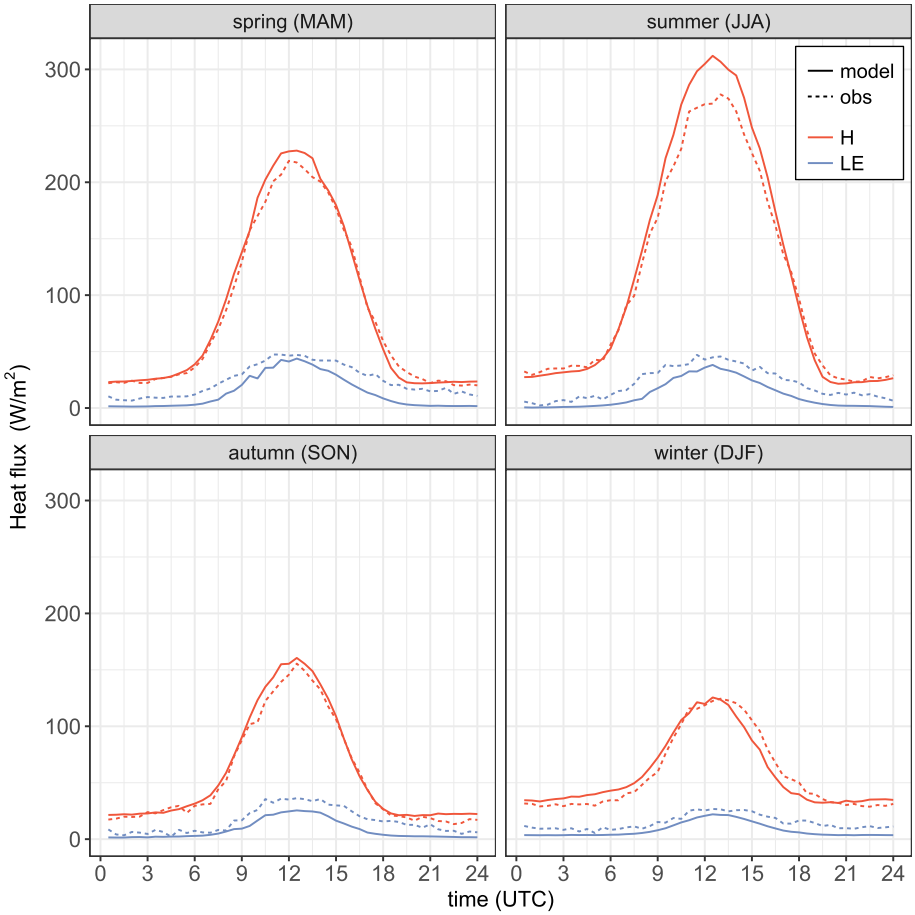

Fig. 7. Seasonal average daily cycle of the observed and modelled turbulent fluxes of sensible (H) and latent (LE) heat.

to frequent door openings. Each time a door is opened, warm indoor air exits the building and is replaced by cold outdoor air. This might increase the building energy consumption related to heating and therefore CO_2 emissions, and this process is not represented in the model. The negative bias of the model in DJF and MAM could be due to the fact that thermal bridges in buildings are not implemented in the model.

The time series of the modelled and observed daily average CO_2 fluxes are displayed in Fig. 9 for the entire year of the CAPITOUL observation campaign. In general, TEB captures the time series of the CO_2 fluxes well but underestimates their temporal variability. Variations in time of the observed footprint area might lead to variability in the observed CO_2 flux that cannot be reproduced by TEB because the modelled area is fixed.

The modelling approach allows the contribution of each source to the total CO_2 flux to be calculated. The most important sources are traffic (48%) and buildings (42%). Human respiration accounts for nearly 10% of the total CO_2 flux. The contribution from urban vegetation is very low (-0.5%). The contribution of each source to the total CO_2 flux strongly fluctuates with the season. In JJA, traffic accounts for more than four-fifths (82%) of the total CO_2 flux, human respiration 17%, buildings 3% and vegetation -2.5%. This highlights the relevance of high-quality traffic data for the modelling of urban CO_2 fluxes. In DJF, the main source of the CO_2 fluxes is buildings (65.7%); traffic accounts for 27.5%, human respiration for 6.5% and vegetation for less than 0.3% of the total flux.

The mean RMSE of the half-hourly modelled CO_2 flux is 15.3 $\mu mol\,m^{-2}\,s^{-1}$. This value is comparable to the model of Crawford and Christen (2015), who used the spatial heterogeneity of their studied site (Sunset, Vancouver, Canada) to calibrate a statistical model for each source and sink of the urban CO_2 flux. Their model was able to predict the half-hourly CO_2 fluxes with an annual RMSE of 12.41 $\mu mol\,m^{-2}\,s^{-1}$, a daytime (from 05 LST to 15 LST) bias of 4 $\mu mol\,m^{-2}\,s^{-1}$ and a night-time (from 22 LST to 04 LST) bias of $-2.5\,\mu mol\,m^{-2}\,s^{-1}$. For Toulouse, TEB simulates a daytime (from 10 UTC to 16 UTC) bias of $-7.1\,\mu mol\,m^{-2}\,s^{-1}$ and a night-time (from 19 UTC to 07 UTC) bias of $-1.4\,\mu mol\,m^{-2}\,s^{-1}$. Järvi et al. (2012) performed a regression between the observed wintertime CO_2 fluxes and the traffic count data for the Kumpula site in Helsinki, Finland. During the winter season, traffic is almost the only source of CO_2 in Helsinki because the ground is covered by snow and the buildings are heated with a district heating system, which does not locally emit CO_2. The RMSE between the predicted CO_2 fluxes from the regression and the observed CO_2 fluxes is 5.24 $\mu mol\,m^{-2}\,s^{-1}$. This is comparable to the RMSE of our model in summer when traffic is the major contributor to the total CO_2 flux. The 7.5 $\mu mol\,m^{-2}\,s^{-1}$ RMSE for Toulouse is of the same order of magnitude as the RMSE found by Järvi et al. (2012).

5. Discussion and conclusions

In this study, we introduced a modelling of the CO_2 fluxes due to buildings, urban vegetation, traffic and human respiration in the urban canopy model TEB. The CO_2 fluxes due to buildings and urban vegetation strongly depend on the prevailing meteorological conditions. For example, the CO_2 flux due to the heating of buildings is highly dependent on air temperature, whereas the CO_2 uptake due to photosynthesis by urban vegetation depends on solar radiation. The contributions of buildings and vegetation to the total CO_2 flux are therefore explicitly modelled using BEM and the ISBA vegetation model. The CO_2 fluxes due to traffic and human respiration are relatively independent of the meteorological conditions. For this reason, simple

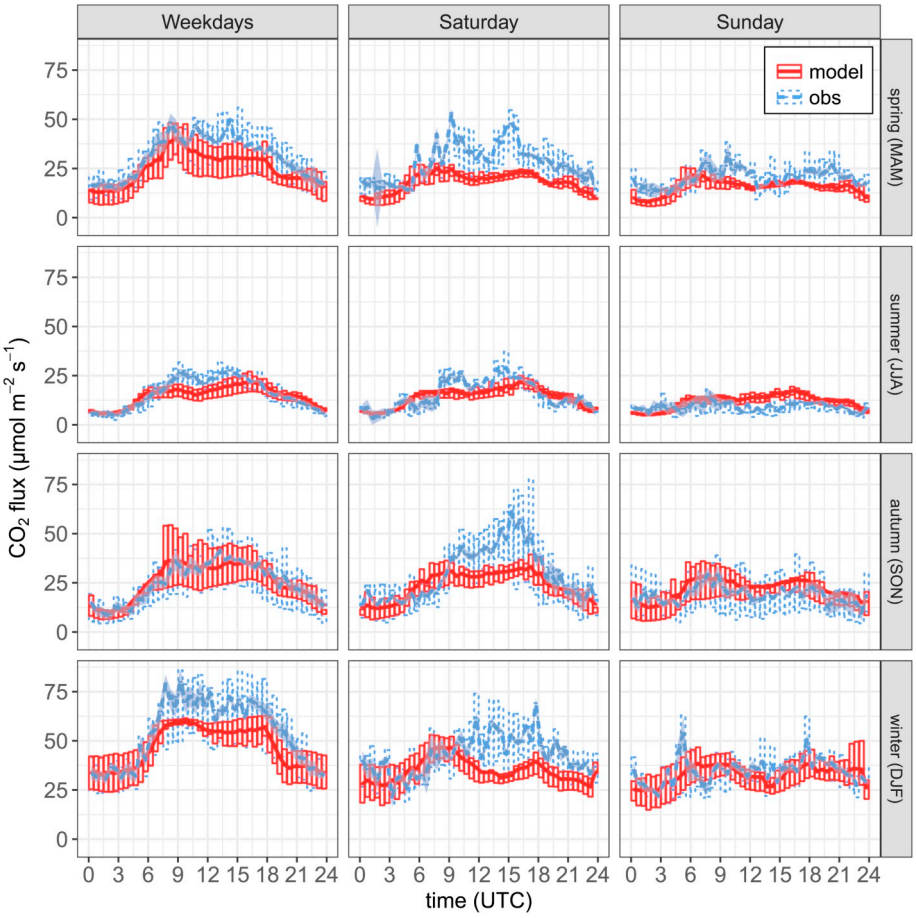

Fig. 8. Mean daily cycle by season for the CO_2 flux. The shading represents the uncertainty associated with the CO_2 flux storage (3.1.3). The boxes show the interquartile range.

parameterisations were implemented in TEB for traffic and human respiration and we assumed that it is not necessary to implement additional detailed parameterisations in TEB because these parameters would not interact with the urban climate modelled by TEB. Users need to specify the annual means for the traffic CO_2 emissions and the average population density. It is also possible to specify modulation factors for the CO_2 emissions due to traffic and human respiration as a function of the hour of the day, the day of the week and the month of the year, as we have done in the present study. Modulation factors and averaged values can be obtained from existing models and inventories such as Agency (2014) for traffic and West et al. (2009) for human respiration.

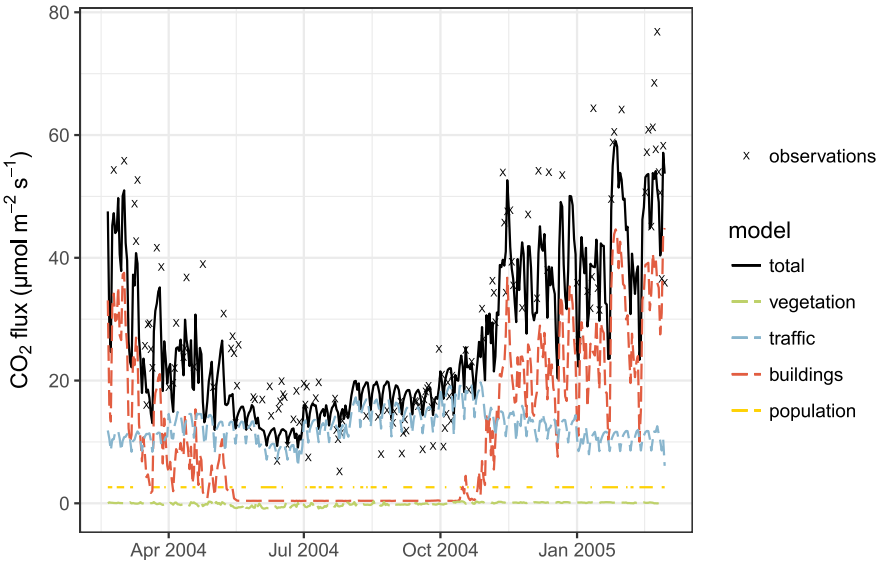

Fig. 9. Times series of the daily average CO_2 fluxes. Observations are plotted when more than 70% of the half-hourly observations are available for a given day.

We investigated the modelled CO_2 fluxes for the centre of Toulouse, a mid-latitude city located in southern France, which is characterised by dense mid-rise (LCZ 2) historical red brick buildings and a strong variety of building uses including offices, commercial establishments, restaurants and residences. The modelled CO_2 fluxes for this area were compared with eddy-covariance measurements made at a pneumatic tower during the CAPITOUL campaign (from February 2004 to February 2005). A sensitivity study indicated that, for the winter season, the modelled CO_2 fluxes strongly depend on data characterising the building equipment (e.g. the type of the heating system), the building use and the human behaviour (e.g. the setpoint temperature for heating). Information concerning the traffic (e.g. fleet composition, number of kilometres travelled and traffic peak time) is also crucial, especially during the summer season when traffic accounts for 83% of the total CO_2 flux at the investigated site. Obtaining such data for any given city of interest worldwide is a major challenge that will need to be addressed by the community. Based on our sensitivity study, we proposed a TEB configuration with a reduced set of input parameters that performs nearly as well as the most detailed configuration. This simpler configuration might be easier to transfer to other cities.

The evaluation of the modelled CO_2 fluxes versus the eddy-covariance measurements provided promising results. TEB, which is independent of the observed CO_2 fluxes, performs similarly to the inverse modelling developed in previous studies based on observations. However, it needs to be kept in mind that evaluations of the urban CO_2 fluxes with eddy-covariance measurements are challenging because these fluxes represent the total CO_2 flux, which is a result of different contributions. In TEB, each contribution is modelled separately and a good model performance for the total CO_2 could be due to error compensations between different contributions (e.g. CO_2 emission due to traffic and CO_2 uptake due to vegetation). An evaluation of TEB for other cities would be beneficial to assess the ability of TEB to model the CO_2 fluxes for a variety of urban areas with different morphologies, building structures, traffic patterns, building uses and behaviours. In particular, the very small relevance of urban vegetation to the total CO_2 fluxes at the CAPITOUL site did not allow any conclusion about the ability of TEB to simulate the CO_2 fluxes due to urban vegetation to be drawn.

This model is a first attempt to implement CO_2 flux modelling in an urban climate model. The different potential improvements to the model include:

- a fluctuating human respiration rate based on the occupation probability of the buildings;
- better vegetation respiration modelling due to the inclusion of a version of ISBA with more vegetation reservoirs (Gibelin et al., 2008); and
- improvements in the building representation in the model, for example, via the implementation of thermal bridges.

In this study, the CO_2 fluxes were modelled for a single grid point representing the centre of Toulouse, France. The advantage of the modelling approach is its extensibility to the city scale as long as we have access to the spatial distribution of the input parameters: the urban morphology (e.g. building density and height), building construction practices, building use, resident behaviour and traffic. TEB can be used to model the spatiotemporal distribution of the CO_2 fluxes with a horizontal resolution of a few hundred meters and a temporal resolution of half an hour. The influence of urban vegetation on the CO_2 fluxes can be investigated by varying their proportions in the model. However, the accuracy of the impact of urban vegetation on the CO_2 fluxes could not be investigated in the present study due to the low plan area density of vegetation in the case study. The modification of the CO_2 fluxes due to changes in the building structure (e.g. the use of insulation materials to reduce the energy demand for heating) or practices related to building use (e.g. a lower setpoint temperature for heating) can be quantified using TEB at the scale of the urban agglomeration.

Code and data availability

The source code of the version of TEB described in this study will be freely available with the next release of SURFEX (SURFEX v9.0) at http://www.umr-cnrm.fr/surfex/. Datasets from the CAPITOUL campaign can be found at http://capitoul.sedoo.fr.

Declaration of interest

The authors declare no conflict of interest.

Acknowledgements

The authors would like to thank William Maurel for his great help in data processing. The authors are grateful to Jennifer Salmond for providing the source code for processing the CO_2 fluxes.

Appendix. ASupplementary data

Supplementary data to this article can be found online at https://doi.org/10.1016/j.aeaoa.2019.100042.

Appendix A. Building Energy Model (BEM)

We modified TEB to consider the latent heat release due to building heating and therefore improve the modelled energy balance. In the previous version of TEB, all energy released by heating was considered to be sensible heat. This energy is now partitioned between sensible heat and latent heat.

The partitioning can be derived from the ratio between the Higher Heating Value (HHV) and the Lower Heating Value (LHV). HHV is the total quantity of energy (latent and sensible) contained in a source of energy. LHV considers only the sensible heat.

The sensible heat consumed can be expressed as

$$H_{cons} = Q_{cons} * \frac{\mathrm{LHV}}{\mathrm{HHV}}, \tag{A.1}$$

where H_{cons} is the sensible energy consumed and Q_{cons} is the total energy consumed. The HHV/LHV ratio depends on the source of energy (SOE) used.

Fractions of buildings heated by a given source of energy (f_{SOE}) and efficiency of heating system are used to rewrite Equation (A.1):

$$H_{cons} = Q_{dem} * \sum_{SOE} \frac{f_{SOE}}{\eta_{SOE}} * \left(\frac{LHV}{HHV}\right)_{SOE}, \tag{A.2}$$

where Q_{dem} is the total energy demand and η_{SOE} is the efficiency of the heating system. In TEB, the efficiency is expressed with respect to the HHV, which means that it is the ratio between the useful heat and the total heat (latent and sensible) contained in the energy source. The consumed latent heat is the difference between the total heat and the sensible heat:

$$LE_{cons} = Q_{dem} * \sum_{SOE} \frac{f_{SOE}}{\eta_{SOE}} * \left(1 - \left(\frac{LHV}{HHV}\right)_{SOE}\right). \tag{A.3}$$

For both forms of consumed heat (H_{cons} and LE_{cons}), we differentiate between demanded heat and waste heat. This is important for the energy balance of TEB because waste heat is rejected outside buildings through the roofs (e.g. chimneys) or walls, whereas demanded heat is injected inside buildings.

For traditional heating systems, only the sensible energy is used to heat the air in the buildings. We therefore consider that all the latent energy consumed by heating is waste heat, leaving us with the following:

$$LE_{waste} = LE_{cons}, \tag{A.4}$$

$$H_{waste} = Q_{cons} - Q_{dem} - LE_{waste}, \tag{A.5}$$

where LE_{waste} and H_{waste} are the latent and sensible energy waste by the heating system, respectively.

Appendix B. Data availability

After the data quality checks, measurements of the CO_2 fluxes based on the eddy-covariance technique were available for more than 50% of the time during each season (Figure B10). The data availability was lowest in winter (51%), which is due to the increased number of precipitation events compared to other seasons. No day of the week was particularly under- or over-represented for any given season or time of the day. We are therefore confident that the shape of the seasonal average daily cycle of the measured CO_2 fluxes is not biased by the availability of the CO_2 flux measurements.

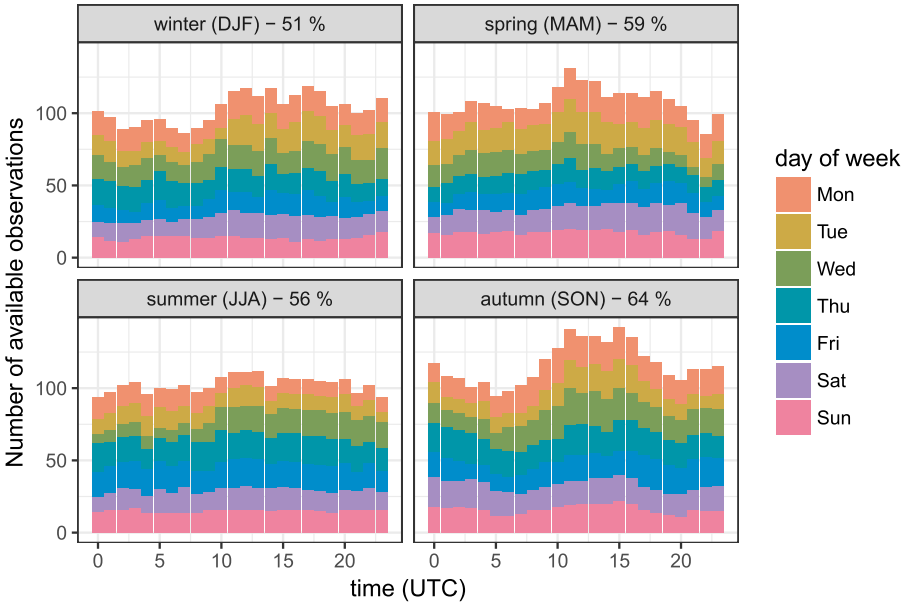

Figure B.10. Availability of CO_2 flux measurements of at least medium quality per season and per day of the week.

Appendix C. Wind rose

The wind rose measured at the mast (Figure C11) is typical of Toulouse, France. The predominant wind directions are southeast and northwest due to wind channelling via the regional topography.

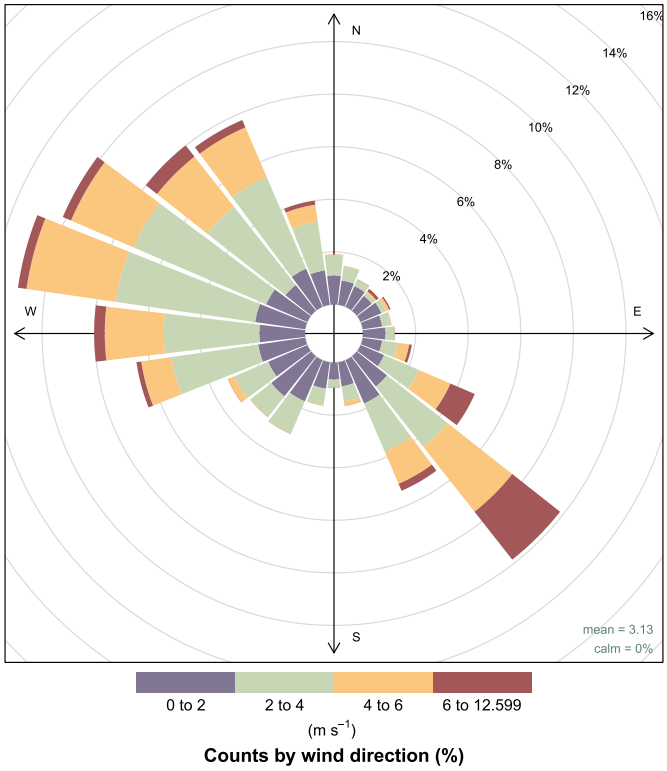

Figure C.11. Wind rose measured at the mast.

Appendix D. Mast position

The mast used for the eddy-covariance measurements has a rated height of 48.05 m above ground level (agl). For safety reasons, it is lowered during strong wind events. Four different heights are used (Table D.6). Observations made at position 2 are rare, and the heights of positions 2 and 3 differ by less than 1 m. For these reasons, measurements at position 2 are considered to have been made at position 3.

Table D.6
Receptor heights for the different positions of the mast.

Mast position	Receptor height (m agl)
1	48.05
2	38.98
3	38.23
4	26.93

In order to analyse only the CO_2 fluxes representative of the local scale, we restricted our analysis to measurements made in the inertial sublayer. Grimmond et al. (2002) advised taking measurements at a minimum of twice the mean building height. Data from position 4 were therefore not analysed.

We further investigated whether observations made at positions 1 or 3 were taken in the inertial sublayer. Two sonic anemometers were mounted on the tower: one at the top of the tower (for the eddy-covariance measurements) and a second a few meters lower (40.01 m for position 1 and 34.03 m for position 3). One feature of the inertial sublayer is that the friction velocity is constant within it. The ratio between the friction velocity measured by the lower and upper anemometers was tested for each mast position (Figure D12). On average, this ratio was around one, which confirms that the measurements were taken in the inertial sublayer.

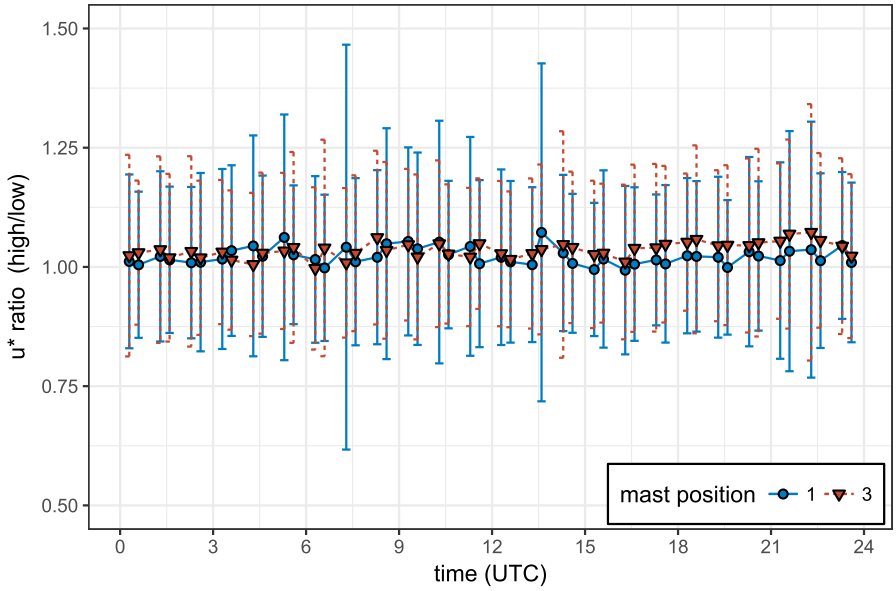

Figure D.12. Mean daily cycle of the ratio between the friction velocity at the upper and lower anemometer positions. The latter were taken at mast positions 1 and 3. The error bars represent one standard deviation.

We also checked whether the data measured at positions 1 and 3 were from the same statistical population. However, a direct comparison of the means, medians or daily cycles of both datasets would not be helpful because measurements at positions 1 and 3 were made during different meteorological situations. For example, the wind speed is higher for the mast position 3 because predicted high-speed winds are the reason for lowering the mast. We therefore investigated the dependency of the CO_2 flux on the wind speed and daily mean temperature for each mast position (Figure D13). For both positions, the measured CO_2 fluxes were very similar; they increased below 15°C and very high values occurred at very low speeds. This finding encouraged us to retain the data from both positions. In this study, the data from positions 1 and 3 were treated as a single dataset.

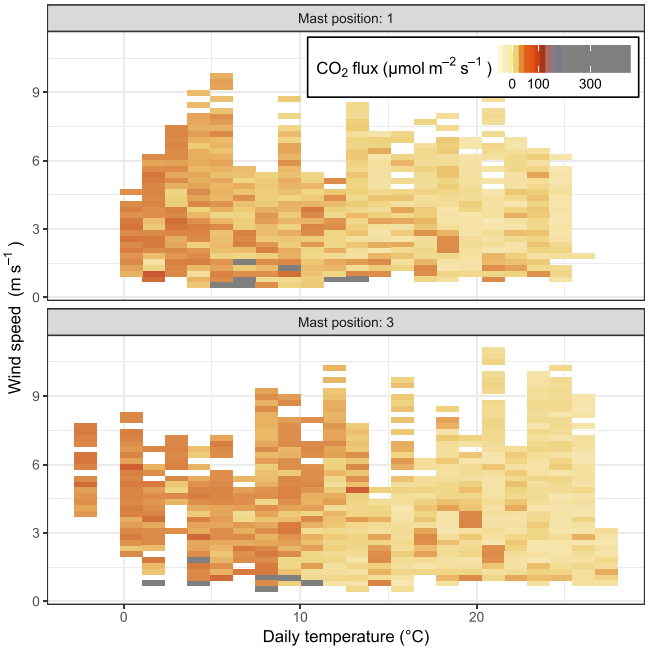

Figure D.13. Measured CO_2 fluxes as a function of the wind speed and daily mean temperature.

Appendix E. Storage

This section describes our methodology for estimating the CO_2 storage below the mast measurement height. For this estimation, we used the half-hourly CO_2 concentration measured at the mast and by two booms at the rooftop level. The booms were located over the two roads adjacent to the building on which the mast was mounted (Rue Alsace-Lorraine and Rue de la Pomme). The measurements of the CO_2 concentrations were taken by two LICOR-7500 instruments placed at a distance of one third of a street width from the building.

The CO_2 concentration variations measured at the mast level can be explained by two physical processes: storage below the mast level or

advection. We estimated the CO_2 storage flux for each 30-min period by assuming that only storage below the mast level (S_STORE) or that only advection (S_ADVEC) was responsible for the CO_2 concentration fluctuations.

We made the following assumptions:

- the CO_2 concentration at the boom level (the roof level) is the mean of the CO_2 concentration measured at the two booms;
- the CO_2 concentration is constant with height between the boom level and the ground level; and
- the CO_2 concentration changes linearly with height between the boom level and the mast level.

First, we assumed that only the advection phenomenon was responsible for the CO_2 fluctuations measured at the mast level. Only the variation of the over-concentration of CO_2 at the boom level compared to the concentration at the mast level is responsible for the storage. The storage at time t is therefore equal to the difference between the volumes P_i and P_{i-1} in Figure E14. The P_i volume depth is f_{canyon} (the fraction of ground not occupied by buildings) below the boom level and 1 above the boom level. This gives the following relationships:

$$P_i = (C_{booms}(t_i) - C_{mast}(t_i))^*\left(z_{booms}{}^*f_{canyon} + \frac{z_{mast} - z_{booms}}{2}\right), \tag{E.1}$$

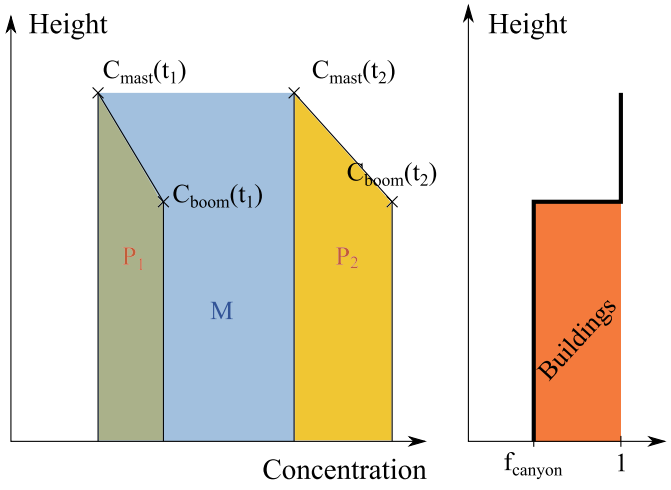

Figure E.14. Illustration of the CO_2 storage calculation method.

$$S\_ADVEC(t) = \frac{(P_i - P_{i-\Delta t})}{\Delta t}, \tag{E.2}$$

where Δt is the time between two measurements (30 min), C_{booms}/C_{mast} is the CO_2 concentration at the boom/mast level and z_{booms}/z_{mast} is the receptor height on the boom/mast.

When we calculate S_STORE, we assume that variations in the concentration at the mast level are due to storage. We therefore need to add the M volume to the previous formula. This gives the following, still considering the shape of the canyon:

$$S\_STORE(t) = \frac{(P_i - P_{i-\Delta t} + M)}{\Delta t}, \tag{E.3}$$

where

$$M = (C_{mast}(t) - C_{mast}(t - \Delta t))^*(z_{booms}{}^*f_{canyon} + z_{mast} - z_{booms}) \tag{E.4}$$

$$= (C_{mast}(t) - C_{mast}(t - \Delta t))^*(z_{booms}{}^*(1 - f_{canyon}) + z_{mast}). \tag{E.5}$$

We calculated the storage according to both methods (S_ADVEC and S_STORE) for each 30-min period. We then retained the maximum (in absolute value) of the two values (hereafter referred to as S_MAX).

When data were not available at the boom level, we assumed that the CO_2 concentration at the boom level was equal to the concentration at the mast level. Then,

$$S\_ADVEC(t) = 0 \tag{E.6}$$

$$S\_STORE(t) = \frac{M}{\Delta t}. \tag{E.7}$$

In this case, the S_STORE formula is equivalent to the formula proposed by Crawford and Christen (2014).

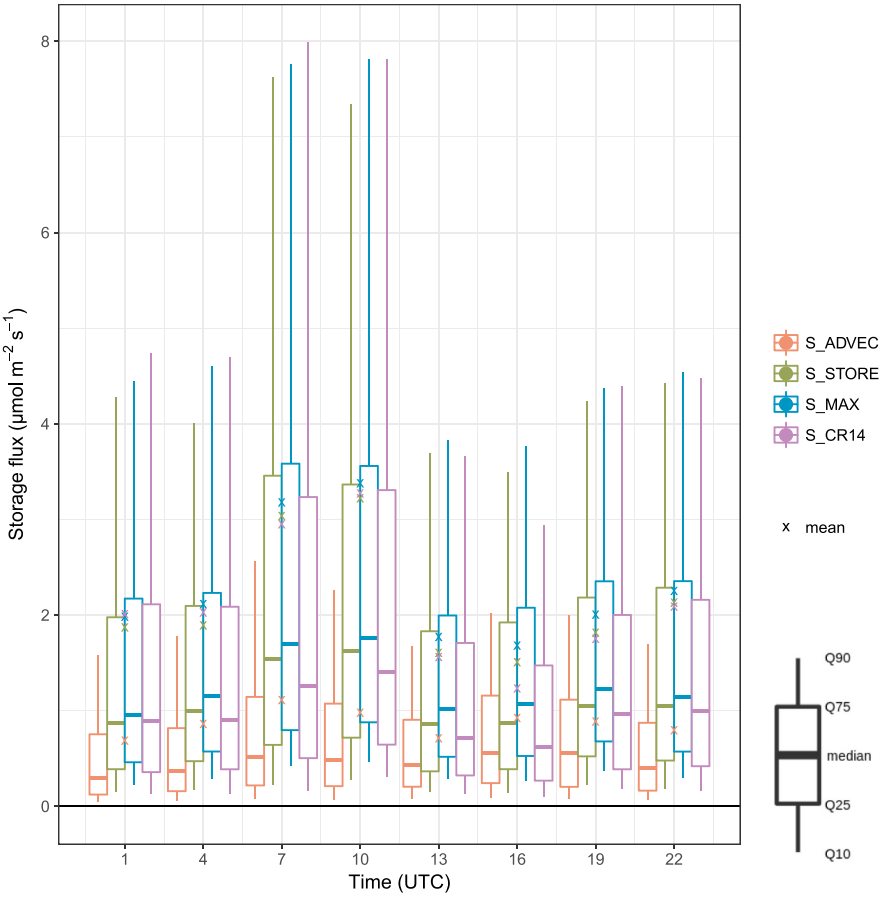

Figure E.15. Storage fluxes for several storage flux calculation methods.

We compared the absolute values of the CO_2 storage flux obtained using the two methods (Figure E15). In general, *S_ADVEC* is lower than *S_STORE*; however, it can be higher. The method for the CO_2 storage flux calculation proposed by Crawford and Christen (2014) (*S_CR*14), which does not require boom level observations, gives lower estimates than *S_MAX*, especially around noon. However, the mean values for *S_STORE*, *S_MAX* and *S_CR*14 are very close. Therefore, the estimation of the CO_2 storage flux obtained with the *S_CR*14 method is regarded as valid for time periods for which no observations at the boom level are available.

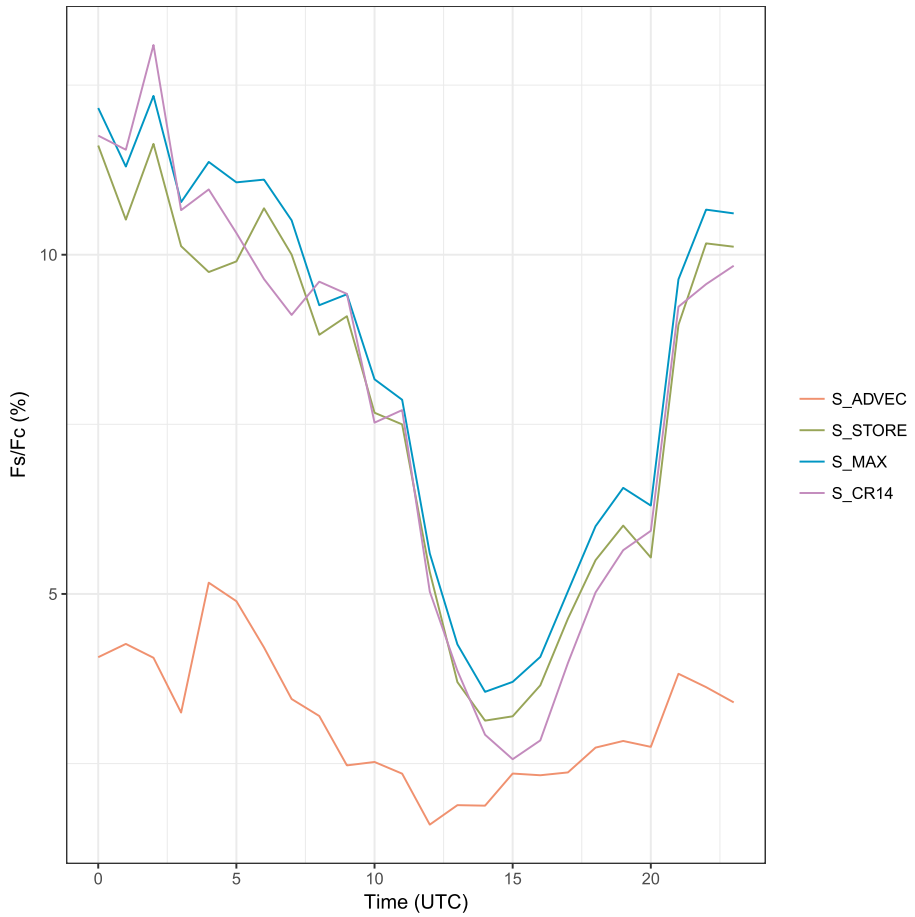

Figure E.16. Daily cycle of the mean absolute CO_2 storage flux divided by the mean absolute CO_2 flux for different methods of estimating the storage flux.

The ratio between the mean absolute CO_2 storage flux and the mean absolute CO_2 flux is very similar for S_STORE, S_MAX and S_CR14 (Figure E16). We retained the S_MAX estimation for the storage calculation.

Appendix F. Simulation parameters

This section provides information on the building construction materials and their physical characteristics (Table F.7), on the urban vegetation characteristics (Table F.8) and on the traffic characteristics (Table F.9) for the area in the centre of Toulouse that was simulated with TEB.

Table F.7
Architectural characteristics of buildings. Parameters are initialised via the database on French building archetypes compiled by Tornay et al. (2017). The centre of Toulouse is dominated by historical (pre-WWII) red brick buildings with tiled roofs that were initially primarily for residential use.

	Material	**Thickness** (m)	**Thermal conductivity** ($W\,m^{-1}K^{-1}$)	**Thermal capacity** ($J\,kg^{-1}K^{-1}$)	**Density** ($kg\,m^{-3}$)	**Albedo**	**Emissivity**
Wall	brick	0.6	0.71	840	1500	0.35	0.9
Roof covering	tile brick	0.02	1.00	837	1700	0.25	0.8
Roof inner layer	plaster, wood	0.02	0.21	850	900	–	0.9
Intermediary floor	wood	0.03	0.23	1600	810	–	0.85
	Glazing type	**Glazing ratio**	**U-Value** ($W\,m^{-2}K^{-1}$)	**Solar heat gain coefficient**			
Windows	single glazing	0.1	4.95	0.6			

Table F.8
Vegetation characteristics.

Parameter	Value
Fraction of high vegetation	0.98
Fraction of low vegetation	0.01
Fraction of bare soil	0.01

(*continued on next page*)

Table F.8 (*continued*)

Parameter	Value
Leaf area index for high vegetation	3.5
Leaf area index for low vegetation	1.0
Height of trees	15 m
Respiration rate of the ecosystem at 25°C	2.2×10^{-7} kg m^{-2} s^{-1}
Cuticular conductance	0.15 mm s^{-1}
Mesophyll conductance (without soil water stress)	1 mm s^{-1}
Maximum air saturation deficit tolerated by vegetation (without soil water stress)	0.1 kg kg^{-1}
Maximum effective life expectancy	365 days

Table F.9
Traffic characteristics. Mean emission factors are calculated from emission factors taken from Hugrel and Joumard (2006).

Mean annual flux density	
Latent flux *LE*	0.8 W m^{-2}
Sensible flux *H*	8 W m^{-2}
CO_2 flux	5.6×10^{-7} kg m^{-2} s^{-1}
Mean emission factors	
Latent heat	471 kJ km^{-1}
Sensible heat	4709 kJ km^{-1}
CO_2	0.47 kg km^{-1}

References

Agency, U.E.P., 2014. MOVES2014 Technical Guidance: Using MOVES to Prepare Emission Inventories for State Implementation Plans and Transportation Conformity. Transportation and Climate Division Office of Transportation and Air Quality Technical report.

Albergel, C., Calvet, J.-C., Gibelin, A.-L., Lafont, S., Roujean, J.-L., Berne, C., Traullé, O., Fritz, N., 2010. Observed and modelled ecosystem respiration and gross primary production of a grassland in southwestern France. Biogeosciences 7 (5), 1657–1668.

Baldocchi, D., Falge, E., Gu, L., Olson, R., others, 2001. FLUXNET: a new tool to study the temporal and spatial variability of ecosystem-scale carbon dioxide, water vapor, and energy flux densities. Bull. Am. Meteorol. Soc. 82 (11), 2415.

Bjorkegren, A.B., Grimmond, C.S.B., Kotthaus, S., Malamud, B.D., 2015. CO2 emission estimation in the urban environment: measurement of the CO2 storage term. Atmos. Environ. 122, 775–790.

Björkegren, A., Grimmond, C., 2018. Net carbon dioxide emissions from central London. Urban Clim. 23, 131–158.

Bocher, E., Petit, G., Bernard, J., Palominos, S., 2018. A geoprocessing framework to compute urban indicators: the MApUCE tools chain. Urban Clim. 24, 153–174.

Boone, A., Masson, V., Meyers, T., Noilhan, J., 2000. The influence of the inclusion of soil freezing on simulations by a soil–vegetation–atmosphere transfer scheme. J. Appl. Meteorol. 39 (9), 1544–1569.

Bourgeois, A., Pellegrino, M., Lévy, J.-P., 2017. Modeling and mapping domestic energy behavior: insights from a consumer survey in France. Energy Res. Soc. Sci. 32, 180–192.

Bueno, B., Pigeon, G., Norford, L.K., Zibouche, K., Marchadier, C., 2012. Development and evaluation of a building energy model integrated in the TEB scheme. Geosci. Model Dev. (GMD) 5 (2), 433–448.

Calvet, J.-C., 2000. Investigating soil and atmospheric plant water stress using physiological and micrometeorological data. Agric. For. Meteorol. 103 (3), 229–247.

Calvet, J.-C., Noilhan, J., Roujean, J.-L., Bessemoulin, P., Cabelguenne, M., Olioso, A., Wigneron, J.-P., 1998. An interactive vegetation SVAT model tested against data from six contrasting sites. Agric. For. Meteorol. 92 (2), 73–95.

Calvet, J.-C., Rivalland, V., Picon-Cochard, C., Guehl, J.-M., 2004. Modelling forest transpiration and CO2 fluxes—response to soil moisture stress. Agric. For. Meteorol. 124 (3–4), 143–156.

Calvet, J.-C., Soussana, J.-F., 2001. Modelling CO2-enrichment effects using an interactive vegetation SVAT scheme. Agric. For. Meteorol. 108 (2), 129–152.

Christen, A., Coops, N.C., Crawford, B.R., Kellett, R., Liss, K.N., Olchovski, I., Tooke, T.R., van der Laan, M., Voogt, J.A., 2011. Validation of modeled carbon-dioxide emissions from an urban neighborhood with direct eddy-covariance measurements. Atmos. Environ. 45 (33), 6057–6069.

Chêne-Pezot, A., 2005. Facteurs d'missions de dioxyde de carbone pour les combustibles. Les chiffres ADEME à utiliser. Technical report, ADEME, Service économie. \url. http://auditenergetique.fr/wa_files/Facteurs_d_emission_CO2_combustibles-2.pdf.

Crawford, B., Christen, A., 2014. Spatial variability of carbon dioxide in the urban canopy layer and implications for flux measurements. Atmos. Environ. 98, 308–322.

Crawford, B., Christen, A., 2015. Spatial source attribution of measured urban eddy covariance CO2 fluxes. Theor. Appl. Climatol. 119 (3–4), 733–755.

Crawford, B., Christen, A., McKendry, I., 2015. Diurnal course of carbon dioxide mixing ratios in the urban boundary layer in response to surface emissions. J. Appl. Meteorol. Climatol. 55 (3), 507–529.

Crawford, B., Grimmond, C.S.B., Christen, A., 2011. Five years of carbon dioxide fluxes measurements in a highly vegetated suburban area. Atmos. Environ. 45 (4), 896–905.

Decharme, B., Boone, A., Delire, C., Noilhan, J., 2011. Local evaluation of the Interaction between Soil Biosphere Atmosphere soil multilayer diffusion scheme using four pedotransfer functions. J. Geophys. Res.: Atmosphere 116 (D20).

Demuzere, M., Harshan, S., Järvi, L., Roth, M., Grimmond, C.S.B., Masson, V., Oleson, K.W., Velasco, E., Wouters, H., 2017. Impact of urban canopy models and external parameters on the modelled urban energy balance in a tropical city. Q. J. R. Meteorol. Soc. 143 (704), 1581–1596.

Edenhofer, O., Pichs-Madruga, R., Sokona, Y., Minx, J.C., Farahani, E., Kadner, S., Seyboth, K., Adler, A., Baum, I., Brunner, S., Eickemeier, P., Kriemann, B., Savolainen, J., Schlömer, S., von Stechow, C., Zwickel, T. (Eds.), 2014. *Climate change 2014: Mitigation of Climate Change ; Working Group III Contribution to the Fifth Assessment Report of the Intergovernmental Panel on Climate Change*. Climate Change 2014. Cambridge Univ. Press, Cambridge, United Kingdom and New York, NY, USA, pp. 892580682 OCLC.

Eggleston, H.S., Buendia, L., Miwa, K., Ngara, T., Tanabe, K., 2006. 2006 IPCC Guidelines for National Greenhouse Gas Inventories. IPCC, Japan Technical report.

Foken, T., Göockede, M., Mauder, M., Mahrt, L., Amiro, B., Munger, W., 2004. Post-field data quality control. In: Handbook of Micrometeorology. Springer, pp. 181–208.

Gibelin, A.-L., Calvet, J.-C., Viovy, N., 2008. Modelling energy and CO2 fluxes with an interactive vegetation land surface model-Evaluation at high and middle latitudes. Agric. For. Meteorol. 148 (10), 1611–1628.

Grimmond, C.S.B., King, T.S., Cropley, F.D., Nowak, D.J., Souch, C., 2002. Local-scale fluxes of carbon dioxide in urban environments: methodological challenges and results from Chicago. Environ. Pollut. 116 (Suppl. 1), S243–S254.

Grimmond, C.S.B., Oke, T.R., 1999. Aerodynamic properties of urban areas derived from analysis of surface form. J. Appl. Meteorol. 38 (9), 1262–1292.

Hugrel, C., Joumard, R., 2006. Directives et facteurs agrégés d'émission des véhicules routiers en France de 1970 à 2025. INRETS Technical report. https://hal.archives-ouvertes.fr/hal-00916989.

Järvi, L., Nordbo, A., Junninen, H., Riikonen, A., Moilanen, J., Nikinmaa, E., Vesala, T., 2012. Seasonal and annual variation of carbon dioxide surface fluxes in Helsinki, Finland, in 2006–2010. Atmos. Chem. Phys. 12 (18), 8475–8489.

Karsisto, P., Fortelius, C., Demuzere, M., Grimmond, C.S.B., Oleson, K.W., Kouznetsov, R., Masson, V., Järvi, L., 2016. Seasonal surface urban energy balance and wintertime stability simulated using three land-surface models in the high-latitude city Helsinki. Q. J. R. Meteorol. Soc. 142 (694), 401–417.

Kljun, N., Calanca, P., Rotach, M.W., Schmid, H.P., 2015. A simple two-dimensional parameterisation for Flux Footprint Prediction (FFP). Geosci. Model Dev. 8 (11), 3695–3713.

Kljun, N., Rotach, M.W., Schmid, H.P., 2002. A three-dimensional backward Lagrangian footprint model for a wide range of boundary-layer stratifications. Boundary-Layer Meteorol. 103 (2), 205–226.

Kordowski, K., Kuttler, W., 2010. Carbon dioxide fluxes over an urban park area. Atmos. Environ. 44 (23), 2722–2730.

Lemonsu, A., Masson, V., Shashua-Bar, L., Erell, E., Pearlmutter, D., 2012. Inclusion of vegetation in the Town Energy Balance model for modelling urban green areas. Geosci. Model Dev. (GMD) 5 (6), 1377–1393.

Liu, H.Z., Feng, J.W., Järvi, L., Vesala, T., 2012. Four-year (2006–2009) eddy covariance measurements of CO2 flux over an urban area in Beijing. Atmos. Chem. Phys. 12 (17), 7881–7892.

Masson, V., 2000. A physically-based scheme for the urban energy budget in atmospheric

models. Boundary-Layer Meteorol. 94 (3), 357–397.
Masson, V., Gomes, L., Pigeon, G., Liousse, C., Pont, V., Lagouarde, J.-P., Voogt, J., Salmond, J., Oke, T.R., Hidalgo, J., Legain, D., Garrouste, O., Lac, C., Connan, O., Briottet, X., Lachérade, S., Tulet, P., 2008. The canopy and Aerosol particles interactions in TOulouse urban layer (CAPITOUL) experiment. Meteorol. Atmos. Phys. 102 (3–4), 135–157.
Masson, V., Le Moigne, P., Martin, E., Faroux, S., Alias, A., Alkama, R., Belamari, S., Barbu, A., Boone, A., Bouyssel, F., Brousseau, P., Brun, E., Calvet, J.-C., Carrer, D., Decharme, B., Delire, C., Donier, S., Essaouini, K., Gibelin, A.-L., Giordani, H., Habets, F., Jidane, M., Kerdraon, G., Kourzeneva, E., Lafaysse, M., Lafont, S., Lebeaupin Brossier, C., Lemonsu, A., Mahfouf, J.-F., Marguinaud, P., Mokhtari, M., Morin, S., Pigeon, G., Salgado, R., Seity, Y., Taillefer, F., Tanguy, G., Tulet, P., Vincendon, B., Vionnet, V., Voldoire, A., 2013. The SURFEXv7.2 land and ocean surface platform for coupled or offline simulation of Earth surface variables and fluxes. Geosci. Model Dev. (GMD) 6, 929–960.
Moriwaki, R., Kanda, M., 2004. Seasonal and diurnal fluxes of radiation, heat, water vapor, and carbon dioxide over a suburban area. J. Appl. Meteorol. 43 (11), 1700–1710.
Nemitz, E., Hargreaves, K.J., McDonald, A.G., Dorsey, J.R., Fowler, D., 2002. Micrometeorological measurements of the urban heat budget and CO2 emissions on a city scale. Environ. Sci. Technol. 36 (14), 3139–3146.
Nieuwstadt, F.T.M., 1981. The steady-state height and resistance laws of the nocturnal boundary layer: theory compared with cabauw observations. Boundary-Layer Meteorol. 20 (1), 3–17.
Noilhan, J., Planton, S., 1989. A simple parameterization of land surface processes for meteorological models. Mon. Weather Rev. 117 (3), 536–549.
Pigeon, G., 2007. *Les échanges surface-atmosphere en zone urbaine - projets Clu-escompte et Capitoul.* PhD thesis. Université Paul Sabatier - Toulouse 3. https://tel.archives-ouvertes.fr/tel-00186764/document.
Pigeon, G., Moscicki, M.A., Voogt, J.A., Masson, V., 2008. Simulation of fall and winter surface energy balance over a dense urban area using the TEB scheme. Meteorol. Atmos. Phys. 102 (3–4), 159–171.
Pigeon, G., Zibouche, K., Bueno, B., Le Bras, J., Masson, V., 2014. Improving the capabilities of the Town Energy Balance model with up-to-date building energy simulation algorithms: an application to a set of representative buildings in Paris. Energy Build. 76 (Suppl. C), 1–14.
Roth, M., Jansson, C., Velasco, E., 2017. Multi-year energy balance and carbon dioxide fluxes over a residential neighbourhood in a tropical city. Int. J. Climatol. 37 (5), 2679–2698.
Satterthwaite, D., 2008. Cities' contribution to global warming: notes on the allocation of greenhouse gas emissions. Environ. Urbanization 20 (2), 539–549.
Schoetter, R., Masson, V., Bourgeois, A., Pellegrino, M., Lévy, J.-P., 2017. Parametrisation of the variety of human behaviour related to building energy consumption in the Town Energy Balance (SURFEX-TEB v. 8.2). Geosci. Model Dev. (GMD) 10 (7), 2801–2831.
Soegaard, H., Møller-Jensen, L., 2003. Towards a spatial CO2 budget of a metropolitan region based on textural image classification and flux measurements. Rem. Sens. Environ. 87 (2–3), 283–294.
Stagakis, S., Chrysoulakis, N., Spyridakis, N., Feigenwinter, C., Vogt, R., 2019. Eddy Covariance measurements and source partitioning of CO2 emissions in an urban environment: application for Heraklion, Greece. Atmos. Environ. 201, 278–292.
Stewart, I.D., Oke, T.R., 2012. Local climate zones for urban temperature studies. Bull. Am. Meteorol. Soc. 93 (12), 1879–1900.
Thomas, C., Foken, T., 2002. Re-evaluation of integral turbulence characteristics and their parameterisations. In: Paper Presented at 15th Symposium on Boundary Layers and Turbulence. Am. Meteorol. Soc., Wageningen, Netherlands.
Tornay, N., Schoetter, R., Bonhomme, M., Faraut, S., Masson, V., 2017. GENIUS: a methodology to define a detailed description of buildings for urban climate and building energy consumption simulations. Urban Clim. 20, 75–93.
U.S. Environmental Protection Agency, 2016. Greenhouse Gas Inventory Guidance. U.S. Environmental Protection Agency Technical report.
Velasco, E., Perrusquia, R., Jiménez, E., Hernández, F., Camacho, P., Rodríguez, S., Retama, A., Molina, L.T., 2014. Sources and sinks of carbon dioxide in a neighborhood of Mexico City. Atmos. Environ. 97, 226–238.
Velasco, E., Roth, M., Tan, S.H., Quak, M., Nabarro, S.D.A., Norford, L., 2013. The role of vegetation in the CO2 flux from a tropical urban neighbourhood. Atmos. Chem. Phys. 13 (20), 10185–10202.
Vesala, T., Järvi, L., Launiainen, S., Sogachev, A., Rannik, U., Mammarella, I., Siivola, E., Keronen, P., Rinne, J., Riikonen, A., Nikinmaa, E., 2008a. Surface–atmosphere interactions over complex urban terrain in Helsinki, Finland. Tellus B 60 (2), 188–199.
Vesala, T., Kljun, N., Rannik, U., Rinne, J., Sogachev, A., Markkanen, T., Sabelfeld, K., Foken, T., Leclerc, M.Y., 2008b. Flux and concentration footprint modelling: state of the art. Environ. Pollut. 152 (3), 653–666.
Vogt, R., Christen, A., Rotach, M.W., Roth, M., Satyanarayana, A.N.V., 2006. Temporal dynamics of CO2 fluxes and profiles over a Central European city. Theor. Appl. Climatol. 84 (1–3), 117–126.
Webb, E.K., Pearman, G.I., Leuning, R., 1980. Correction of flux measurements for density effects due to heat and water vapour transfer. Q. J. R. Meteorol. Soc. 106 (447), 85–100.
Weissert, L., Salmond, J., Turnbull, J., Schwendenmann, L., 2016. Temporal variability in the sources and fluxes of CO2 in a residential area in an evergreen subtropical city. Atmos. Environ. 143, 164–176.
West, T.O., Marland, G., Singh, N., Bhaduri, B.L., Roddy, A.B., 2009. The human carbon budget: an estimate of the spatial distribution of metabolic carbon consumption and release in the United States. Biogeochemistry 94 (1), 29–41.
Yang, Bai, Hanson Paul, J., Riggs Jeffery, S., Pallardy Stephen, G., Mark, Heuer, Hosman Kevin, P., Meyers Tilden, P., Wullschleger Stan, D., Gu, Lian-Hong, 2007. Biases of CO2 storage in eddy flux measurements in a forest pertinent to vertical configurations of a profile system and CO2 density averaging. J. Geophys. Res.: Atmosphere 112 (D20).